Why $\langle S \rangle$?

Because electron spin relaxation, i.e., jumps between the various eigenstates of the spin Hamiltonian, can be extremely rapid.

If jump rates are <u>slow</u> compared with Larmor precession rate of nuclear moments in the presence of the <u>internal</u> magnetic field, which in turn is faster than the decay rate of the nuclear excited state ($10^7 s^{-1}$), then each occupied spin state <u>contributes</u> <u>individually</u> to overall magnetic hyperfine pattern with a Mössbauer pattern weighted by the corresponding Boltzmann factor.

If the jump rates among the eigenstates of the spin Hamiltonian are <u>rapid</u> compared with the rate of Larmor precession of the nuclear moments in the presence of the <u>internal</u> magnetic field, then only the thermal average of the spin expectation values can be sampled, namely

$$\langle S_i \rangle_{av} = \sum_j \langle S_i \rangle_j \exp(-E_j/kT) \Big/ \sum_j \exp(-E_j/kT)$$

The Larmor precession times of the nuclear moments here must also be shorter than the mean lifetime of the nuclear excited state ($1.4 \times 10^{-7} s$)

In the slow relaxation limit, we may write for each occupied spin state $\sim a \vec{I} \cdot \vec{S}$. If there is only one such state, then we expect the following nuclear energy level pattern and Mössbauer spectrum.

$S = \frac{1}{2}$

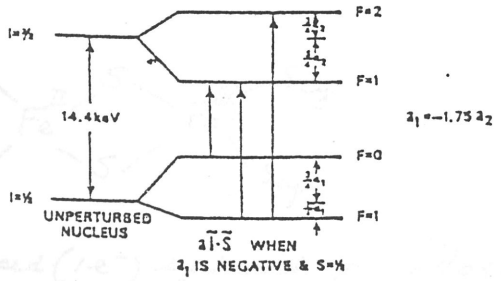

EFFECT OF MAGNETIC HYPERFINE INTERACTION ON NUCLEAR LEVELS

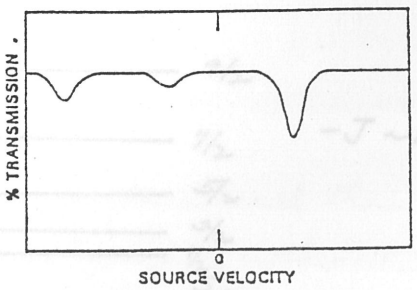

RESULTING MOSSBAUER SPECTRUM

To obtain energies, note that

$$\vec{F} = \vec{I} + \vec{S} \quad \text{and} \quad F^2 = (\vec{I}+\vec{S})\cdot(\vec{I}+\vec{S})$$

$$\therefore F^2 - I^2 - S^2 = 2\vec{I}\cdot\vec{S}$$

$$\text{or } \langle \vec{I}\cdot\vec{S} \rangle = \tfrac{1}{2}\left[F(F+1) - I(I+1) - S(S+1) \right]$$

$$\text{and } a\langle \vec{I}\cdot\vec{S} \rangle = \frac{a}{2}\left[F(F+1) - I(I+1) - S(S+1) \right]$$

Excited state $I = 3/2$, $S = 1/2$ $\therefore F = 2$ and 1

Energy levels $F=2$: $\langle a\vec{I}\cdot\vec{S} \rangle = \frac{a}{2}\left[2(2+1) - \left(\frac{3}{2}\right)\left(\frac{3}{2}+1\right) - \frac{1}{2}\left(\frac{1}{2}+1\right) \right]$

$$= 3/4\, a$$

$F=1$: $\langle a\vec{I}\cdot\vec{S} \rangle = \frac{a}{2}\left[1(1+1) - \left(\frac{3}{2}\right)\left(\frac{3}{2}+1\right) - \frac{1}{2}\left(\frac{1}{2}+1\right) \right]$

$$= -\frac{5}{4}a$$

Ground state $I = 1/2$, $S = 1/2$ $\therefore F = 1, 0$

Energy levels $F=1$: $\langle a'\vec{I}\cdot\vec{S} \rangle = \frac{a'}{2}\left[(1)(2) - \left(\frac{1}{2}\right)\left(\frac{1}{2}+1\right) - \frac{1}{2}\left(\frac{1}{2}+1\right) \right]$

$$= \frac{a'}{4}$$

$F=0$: $\langle a'\vec{I}\cdot\vec{S} \rangle = \frac{a'}{2}\left[(0)(0+1) - \frac{1}{2}\left(\frac{1}{2}+1\right) - \frac{1}{2}\left(\frac{1}{2}+1\right) \right]$

$$= -\frac{3}{4}a'$$

Slow relaxation limit usually achieved at low temperatures (4.2K) and high $\vec{H}_{external}$ (augment $\vec{H}_{ee}$)

Rapid relaxation limit obtains at high temperatures and zero $\vec{H}_{external}$

Example from Ferredoxin literature

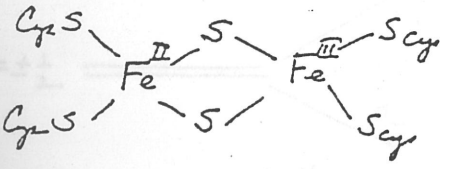

reduced ($1e^-$) spinach ferredoxin

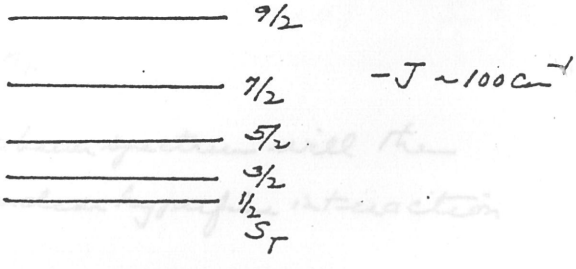

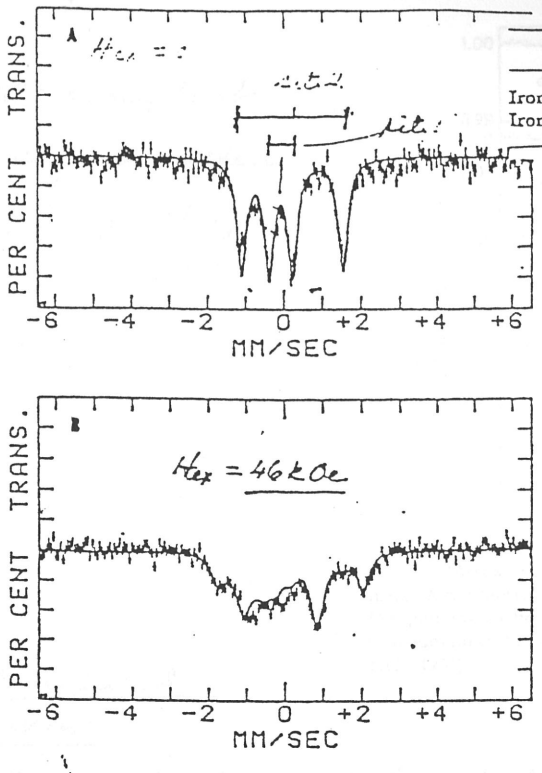

Mössbauer spectra and computed Mössbauer spectra for reduced spinach ferredoxin at 256 °K. (a) Lyophilized spinach ferredoxin in zero magnetic field; (b) Lyophilized spinach ferredoxin with 46 kG magnetic field parallel to gamma-ray direction. Velocities relative to platinum source

Mössbauer parameters for the high temperatur... PNR spectra

	IS/Pt (mm/S)	Q	η
Iron Site # 1	−0.10	+	0.5
Iron Site # 2	+0.19	−	0 to 0.5

At high temperatures,

$\langle S_z \rangle = 0$

→ Two quadrupole doublets

{ 1 high spin Fe(III) site #1
{ 1 high spin Fe(II) site #2

← Application of magnetic field to create electron spin alignment ($\langle S_z \rangle \neq 0$) for a paramagnetic system

Example from the heme protein literature

Cytochrome c Peroxidase fluoride

high spin ferric heme $S = 5/2$

$D \cong 7\ cm^{-1}$

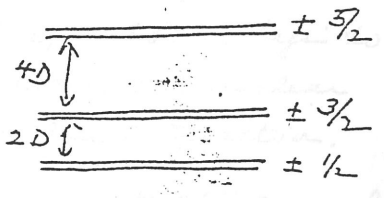

At low temperature, say 4K, only ± ½ appreciably populated and these states are degenerate. So $\langle S_z \rangle = 0$

However, the application of a small magnetic field (~100 G) can be used to align the electronic magnetic moments, i.e., create an electron polarization, so that $\langle S_z \rangle \neq 0$

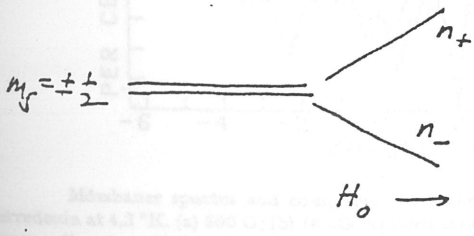

$n_- > n_+$

and the Mössbauer spectrum will then exhibit nuclear hyperfine interaction

Excellent example of well-defined nuclear hyperfine splitting in a hemoprotein -

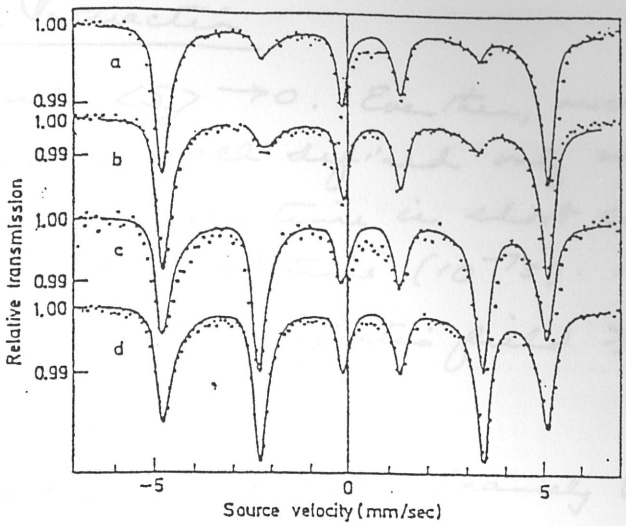

Mössbauer spectra of cytochrome *c* peroxidase fluoride; (a) — proto, (b) — meso. A magnetic field of 100 G is applied parallel to the direction of observation of the gamma-ray beam; (c) — proto, (d) — meso. A magnetic field of 500 G is applied perpendicular to the direction of observation of gamma-ray beam. (After Lang, Ref. (125)).

Return to reduced ferredoxin

Note that in the case of reduced spinach ferredoxin, a much higher polarizing magnetic field (> 30 kOe) was required before distinct Mössbauer spectra could be discerned for the two electron spin populations in this $S = 1/2$ system ($m_S = \pm 1/2$).

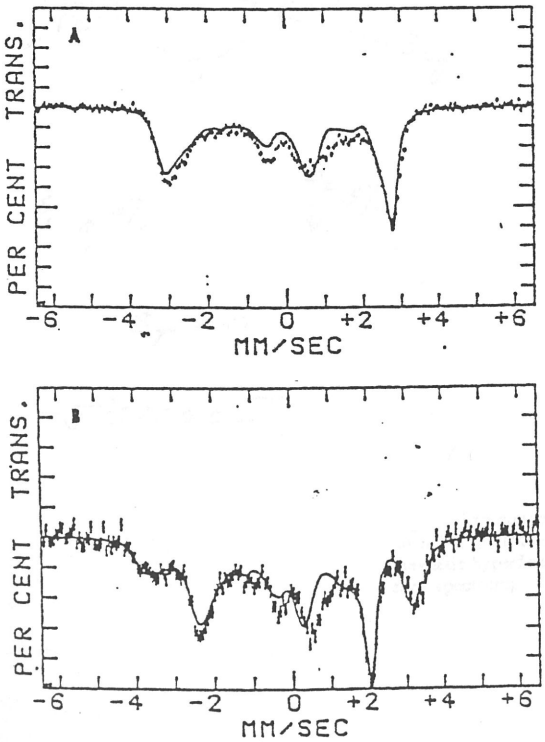

Mössbauer spectra and computed Mössbauer spectra for reduced spinach ferredoxin at 4.3 °K. (a) 580 G; (b) 46 kG. Applied magnetic fields are parallel to gamma-ray direction. Velocities are relative to platinum source matrix. Boltzmann weighting factor for electronic states = — 0.26

Here, at 580 G, begin to see evidence of nuclear hyperfine interaction. But only at 46 kOe and 4.2 K, differences in the population of the two states become measurable by Mössbauer spectroscopy

$+\frac{1}{2}$ $n_+ = 0.26$ ↓

$-\frac{1}{2}$ $n_- = 1.0$ ↑

m_S

$S_T = 1/2$

→ (4) Nuclear Zeeman Interaction

Important only when $\langle S_z \rangle \to 0$. Even then, nuclear magnetic energy states are well defined only when the nuclear Larmor precession time is short compared with the nuclear radiative lifetime (10^{-7}s). This implies an externally applied magnetic field ≥ 30 kOe for ^{57}Fe.

The sign of the quadrupole splitting (namely V_{zz}) and the value of the asymmetry parameter can be found by applying a large (30–50 kG or 3–5 Tesla) magnetic field to the sample and determining whether $m_I = \pm 3/2$ states lie higher or lower in energy than the $m_I = \pm 1/2$ states in the excited isomeric state.

Example from Ferredoxin literature

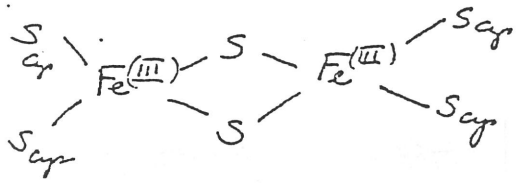

$S_1 \uparrow 5/2$ $\quad$ $S_2 \downarrow 5/2$

$S_T = 0$

$-J \geq 100\ cm^{-1}$

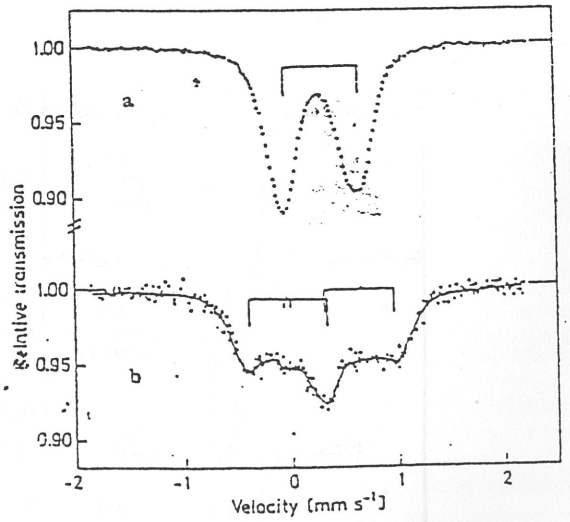

Experimental Mössbauer spectra of *Euglena* ferredoxin (a) at 4.2 K in zero-applied field and (b) in 3 T-applied field, perpendicular to the γ-beam. The solid line represents a simulation with zero-magnetic hyperfine contribution; i.e. the magnetic splitting arises solely from the applied field (see stick-spectrum).

Oxyferryl

Mössbauer Characteristic $\delta(\alpha\text{-Fe}) \sim 0.05$ mm/s

Mössbauer parameters of porphyrin complexes containing Fe(IV)

Compound	T(K)/matrix	$\delta(\alpha\text{-Fe})$ (mms^{-1})	ΔE_Q (mms^{-1})	Ref.
$[(TMP)Fe{=}O]^+(Cl^-)$	77/toluene/methanol (4:1)	0.06	1.62	[175]
	4.2/toluene/methanol (4:1)	0.08	1.62	
$[(TMP)Fe{=}O]^+(OSO_2CF_3)$	4.2/toluene	0.08	1.62	[176]
$[TPP(2,6\text{-Cl})Fe{=}O]^+(OSO_2CF_3)$	4.2/CH_3CN	0.08	1.80	
(TPP)Fe=O/1-methylimidazole	4.2/toluene	0.11	1.26	[b]
(TPP)Fe=O/pyridine	4.2/toluene	0.10	1.56	
$(TP_{piv}P)Fe{=}O$/tetrahydrofuran	4.2/tetrahydrofuran	0.12	2.20	[c]
$(TP_{piv}P)Fe{=}O$/1-methylimidazole	4.2/tetrahydrofuran	0.109	1.372	
(TMP)Fe=O	nd/nd	0.04	2.3	[d]
TPP(2,6-Cl)Fe=O/tetrahydrofuran	4.2/tetrahydrofuran	0.09	2.08	[e]
TPP(2,6-Cl)Fe=O/dimethylformamide	4.2/dimethylformamide	0.09	1.81	
TPP(2,6-Cl)Fe=O/1-methylimidazole	4.2/tetrahydrofuran	0.07	1.35	
Compound ES cytochrome c peroxidase	4.2/H_2O	0.05	1.55	[f]
$(TMP)Fe(OCH_3)_2$	4.2/toluene	−0.022	2.17	[g]
Horse-radish peroxidase I	−[a]/glycerol/H_2O(1:1)	0.08	1.25	[179]
Horse-radish peroxidase II	77/H_2O	0.03	1.36	[h]
Chloroperoxidase I	4.2/peracetic acid	0.15	1.02	[102]

[a] Parameters derived from simulations of temperature-dependent and field-dependent Mössbauer spectra.
[b] Simonneaux et al. (1982) Biochim. Biophys. Acta 716:1.
[c] Schappacher et al. (1985) J. Am. Chem. Soc. 107:3736.
[d] Groves et al. (1986) Inorg. Chem. 25:123.
[e] Gold et al. (1988) J. Am. Chem. Soc. 110:5756.
[f] Lang et al. (1976) Biochim. Biophys. Acta, 451:250.
[g] Groves et al. (1985) J. Am. Chem. Soc. 107:354.
[h] Moss et al. (1969) Biochemistry 8:4159

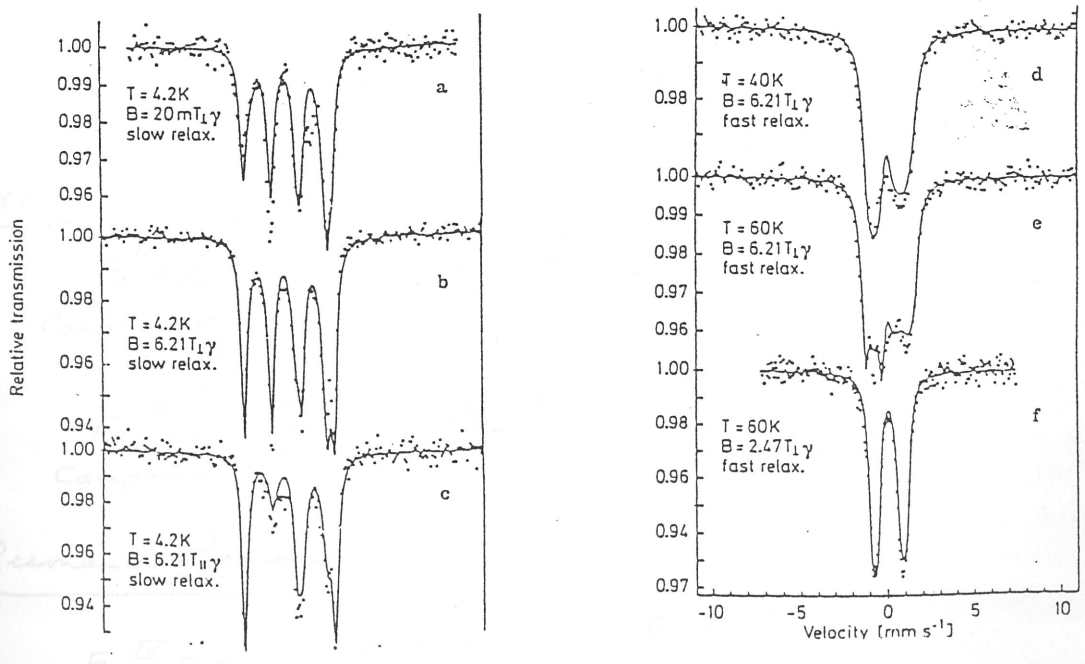

Experimental Mössbauer spectra of $[(TMP)Fe{=}O]^+$ (Cl^-) at various temperatures and applied fields as indicated. The *solid lines* are simulated spectra with the parameters given in Table 8. Taken from [9]

EPR

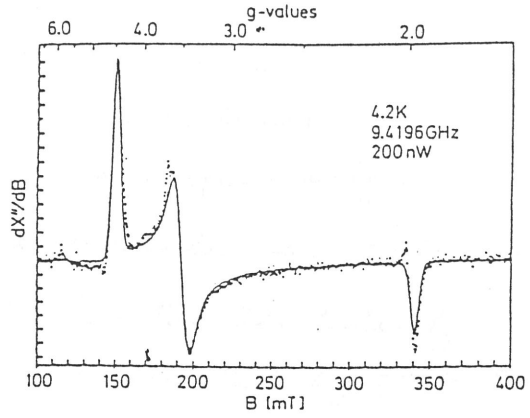

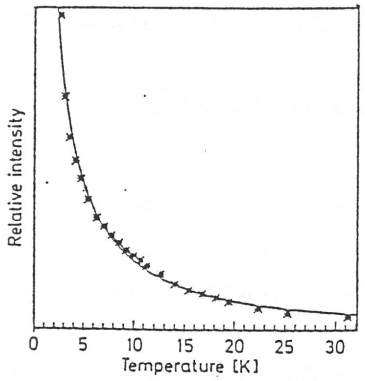

.. EPR spectrum of [(TMP) Fe = O]$^+$ Cl^-) in toluene/methanol (4 : 1) at 4.2 K. The *solid line* is a simulation of a powder spectrum based on the approximation of a Kramers doublet with effective spin $S^{eff} = 1/2$ and effective g-values $g_x^{eff} = 4.47$, $g_y^{eff} = 3.50$, and $g_z^{eff} = 1.98$. (b) Temperature dependence of EPR signal. Taken from [176]

S_1 (Fe IV) = 1

S_2 ($P^{+\cdot}$) = 1/2

S_T = 3/2 ground state

.. ring ferromagnetic coupling

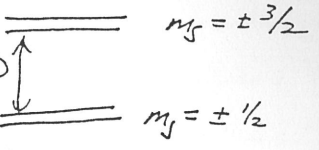

EPR ←

EPR intensity → D ~ 6 - 12 cm^{-1} (positive)

Simulation of Mössbauer → D = +6.2 ± 2 cm^{-1}

EXAFS

$Fe^{IV}=O$ ~ 1.65 Å

Compound II

$Fe^{IV}=O$ $P^{+\cdot}$ ~ 1.65 Å

Compound I

Resonance Raman

$Fe^{IV}=O$ stretch 790 cm^{-1}

sensitive to $^{16}O/^{18}O$

Iron-sulfur proteins

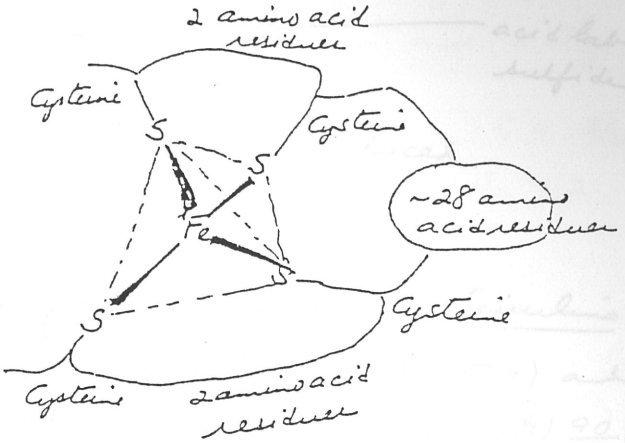

→ Rubredoxin

* 1 iron atom
* four cysteines
* no inorganic sulfur
* Molecular mass ~ 6000
* Fe atom tetrahedrally coordinated by four cysteine-sulfur atoms
* Tetrahedron is markedly distorted
* Fe-S distances (±0.05 A°) 2.39, 2.33, 2.31, 1.97 A°
* S-Fe-S angles range between 101° and 118°
* First isolated from C. pasteurianum
* Crystal structure known (J. Mol. Biol (1970) 50, 391; JACS (1971) 93 1810)
* Crystal structure of enzyme from the extreme thermophilic archaebacterium ES-4 was also reported by M. Day, ... M. Adams & D. Rees Prot. Science (1992) 1, 1494.

Plant 2Fe 2S

→ Ferredoxins

* 2Fe 2S iron sulfur cluster anchored to polypeptide by ligation to 4 cysteine sulfur atoms
* 12,000 - 24,000 in molecular mass
* Occur in all green plants, algae, photosynthetic bacteria and protozoa, and some fermentative anaerobic bacteria
* participates in biological electron transfer toward low-potential end of the photosynthetic process.

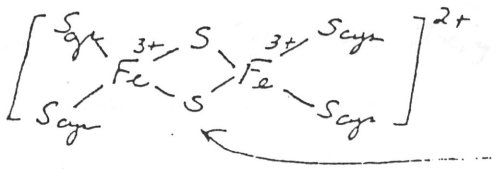

oxidized

acid labile sulfide

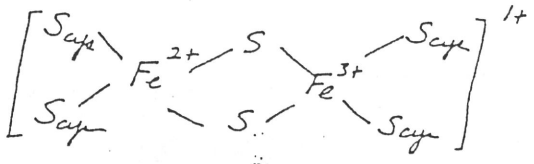

1e⁻ reduced

* Crystal structures known for ferredoxins from Spirulina platensis (K. Fukuyama et al., Nature (1980) 286, 522-524) and from Aphanothece sacrum (T. Tsukihara, J. Biochem. (1981) 90, 1763-1773); isolation of model compounds preceded x-ray structure

* Redox potentials: −240 to −420 mV (E_0', pH = 7.0)

	Fe	S=	Electrons Transferred	MW	E_0' (mV)	EPR g-values
Azotobacter Fe—S Protein I	2	2	1	21,000	−300 to −400[a]	$g_x = 1.93$ $g_y = 1.95$ $g_z = 2.02$
Azotobacter Fe—S Protein II	2	2	1	24,000	−300 to −400[a]	$g_x = 1.90$ $g_y = 1.95$ $g_z = 2.05$
Parsley Ferredoxin	2	2	1	12,000	−300 to −400[a]	$g_x = 1.89$ $g_y = 1.96$ $g_z = 2.05$
Adrenodoxin	2	2	1	12,000	−370	$g_x = 1.93$ $g_y = 1.94$ $g_z = 2.02$
Spinach Ferredoxin	2	2	1	12,000	−420	$g_x = 1.89$[b] $g_y = 1.96$[b] $g_z = 2.05$[b]
C. Pasteurianum Paramagnetic Protein	2	2	1	24,000	−300 to −400[a]	$g_x = 1.93$ $g_y = 1.95$ $g_z = 2.00$

Spinach ferredoxin (reduced) 20°K

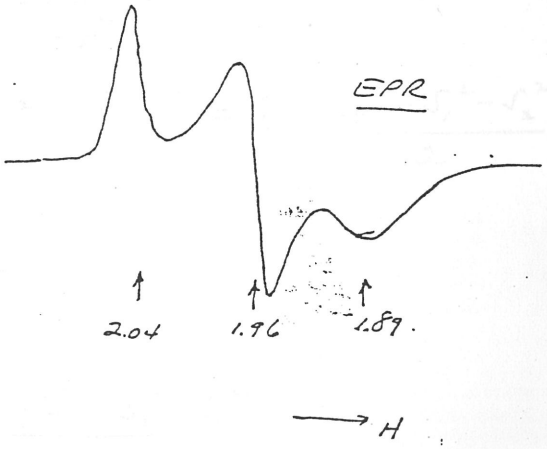

* all ferredoxins display $g_{av} = 1.94$ EPR when reduced by 1e⁻. The oxidized forms of the proteins are diamagnetic

* $[Fe_2S_2]^{2+}$ $[Fe_2S_2]^{1+}$

$-J$: 150 cm⁻¹ 100 cm⁻¹ (X)

Fe···Fe increases by 0.1 Å

* The EPR g-values ($g_z - 2$, $g_{x,y} < 2$) observed for mixed valence clusters a consequence of antiferromagnetic exchange coupling between a high-spin ferric ion and a high-spin ferrous ion.

$S_1 = 5/2$

$S_2 = 2$

Vector model for coupling of the two spins:

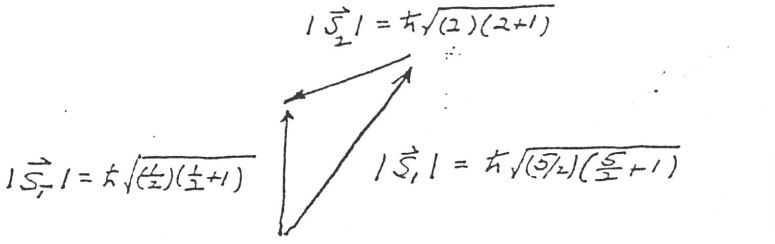

Define $\vec{\mu} = (\mu_x \ \mu_y, \mu_z)$
$= -(g_x \ g_y \ g_z)\beta \vec{S}_T$

From this, it follows that

$$\underset{\sim}{g}\vec{S}_T = \underset{\sim}{g}_1 \frac{\vec{S}_1 \cdot \vec{S}_T}{\vec{S}_T} + \underset{\sim}{g}_2 \frac{\vec{S}_2 \cdot \vec{S}_T}{\vec{S}_T}$$

$$\text{or } \underset{\sim}{g} = \underset{\sim}{g}_1 \frac{\vec{S}_1 \cdot \vec{S}_T}{S_T^2} + \underset{\sim}{g}_2 \frac{\vec{S}_2 \cdot \vec{S}_T}{S_T^2}$$

Now $\vec{S}_1 \cdot \vec{S}_T = \vec{S}_1 \cdot (\vec{S}_1 + \vec{S}_2) = S_1^2 + \vec{S}_1 \cdot \vec{S}_2 = S_1^2 + \frac{S_T^2 - S_1^2 - S_2^2}{2}$

$$= \frac{S_T^2 + S_1^2 - S_2^2}{2}$$

Similarly $\vec{S}_2 \cdot \vec{S}_T = \frac{S_T^2 + S_2^2 - S_1^2}{2}$

$$\therefore \underset{\sim}{g} = \underset{\sim}{g}_1 \frac{S_T^2 + S_1^2 - S_2^2}{2S_T^2} + \underset{\sim}{g}_2 \frac{S_T^2 + S_2^2 - S_1^2}{2S_T^2}$$

$$= \underset{\sim}{g}_1 \cdot \frac{(S_T)(S_T+1) + S_1(S_1+1) - S_2(S_2+1)}{2(S_T)(S_T+1)} + \underset{\sim}{g}_2 \frac{(S_T)(S_T+1) + (S_2)(S_2+1) - S_1(S_1+1)}{2(S_T)(S_T+1)}$$

$$= \underset{\sim}{g}_1 \cdot \frac{7}{3} + g_2 \cdot (-\frac{4}{3}) = \frac{1}{3}(7g_1 - 4g_2)$$

or

$$g_x = \frac{1}{3}(7g_{1x} - 4g_{2x})$$
$$g_y = \frac{1}{3}(7g_{1y} - 4g_{2y})$$
$$g_z = \frac{1}{3}(7g_{1z} - 4g_{2z})$$

For high spin ferric

$S_1 = 5/2$

$g_{1x} \cong g_{1y} \cong g_{1z} = 2.0$

For high spin Ferrous ion $S_2 = 2$

and $g_{2x} = g_e - \frac{6\lambda}{\Delta_{yz}}$ $(\lambda < 0)$

$g_{2y} = g_e - \frac{6\lambda}{\Delta_{xz}}$

$g_{2z} = g_e$

distorted tetrahedron

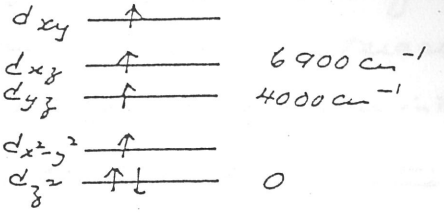

For spinach ferredoxin, calculated values are

$g_{2x} = 2.12$, $g_{2y} = 2.07$, and $g_{2z} = 2.00$

Therefore

$g_x = \frac{1}{3}(7 \times 2.0 - 4 \times 2.12) = 1.84$

$g_y = \frac{1}{3}(-7 \times 2.0 - 4 \times 2.07) = 1.91$

$g_z = \frac{1}{3}(7 \times 2.0 - 4 \times 2.00) = 2.00$

$g_{av} = 1.92$

* Mössbauer of oxidized Ferredoxins ($[Fe_2S_2]^{2+}$)

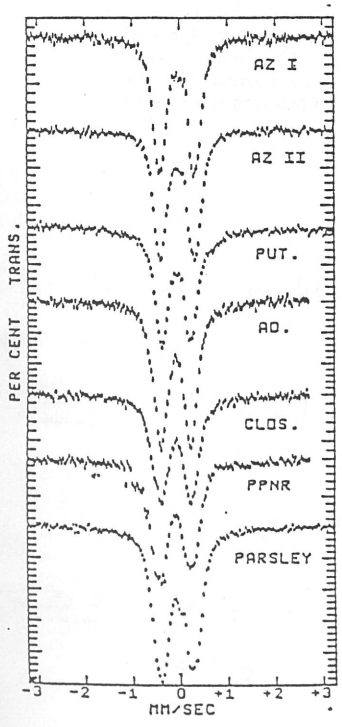

Mössbauer spectra of oxidized plant-type iron-sulfur proteins in zero applied magnetic field. Abbreviations: AZI = *Azotobacter Fe-S* protein I, 4.6 °K; AZII = *Azotobacter* Fe-S protein II, 4.2 °K; Put. = Putidaredoxin, 4.2 °K; Ad. = Pig Adrenodoxin, 4.2 °K; Clos. = Clostridial paramagnetic protein, 4.2 °K; PPNR = Spinach ferredoxin, 4.5 °K; Parsley = Parsley Ferredoxin, 4.2 °K. Velocity scale is relative to iron in platinum

1 quadruple doublet

$\Delta E_Q = QS \cong 0.77$ mm/s (independent of temperature below 250K)

$\delta(\alpha\text{-Fe}) = 0.2$ mm/s at 4.2K (characteristic of high-spin ferric ions tetracoordinated to sulfur ligands)

2 slightly different doublets in Rieske protein (1/3 the Fe has one histidine as ligand instead of cysteine)

For this second site $QS \cong 0.9$ mm/s

$\delta(\alpha\text{-Fe}) \cong 0.3$ mm/s

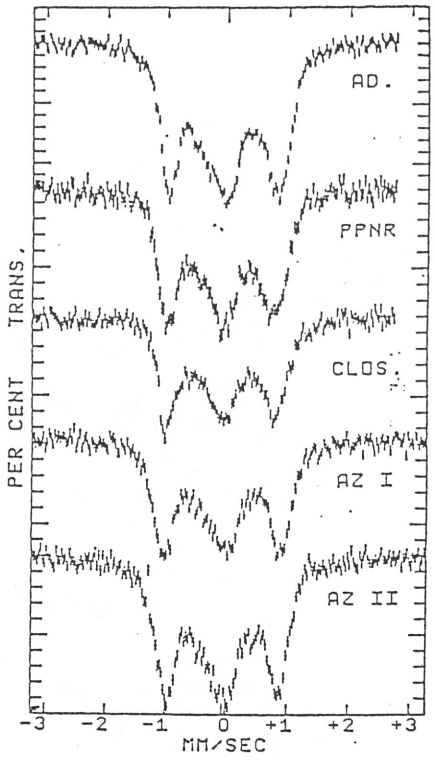

Mössbauer spectra of oxidized plant-type iron-sulfur proteins in high applied magnetic field. Abbreviations: Ad. = Pig Adrenodoxin, 4.2 °K, 46 kG; PPNR = Spinach Ferredoxin, 4.5 °K, 50 kG; Clos. = Clostridial Paramagnetic Protein, 4.2 °K, 46 kG; AZI = *Azotobacter* Fe-S Protein I, 4.6 °K, 46 kG; AZII = *Azotobacter* Fe-S Protein II, 4.2 °K, 46 kG. Applied magnetic field is parallel to gamma-ray direction

broadening of doublet from nuclear Zeeman interaction; NO magnetic hyperfine interaction ∴ cluster is diamagnetic

* Mössbauer of 1-e⁻ reduced ferredoxin ($[Fe_2S_2]^{1+}$)

Experimental Mössbauer spectra of reduced spinach ferredoxin. *Solid lines* are simulations, i.e. (c) for Fe(III) $S_z = -1/2$, (d) for Fe(III) $S_z = +1/2$, (e) for Fe(II) $S_z = -1/2$, (f) for Fe(II) $S_z = +1/2$, (g) Boltzmann-weighted sum of (c), (d), (e) and (f), superimposed over experimental spectrum. Taken from [76]. (Zero-velocity given relative to Pt-source matrix; transformation of δ(Pt) to δ(α-Fe) is provided by adding 0.349 mms^{-1} to δ(Pt))

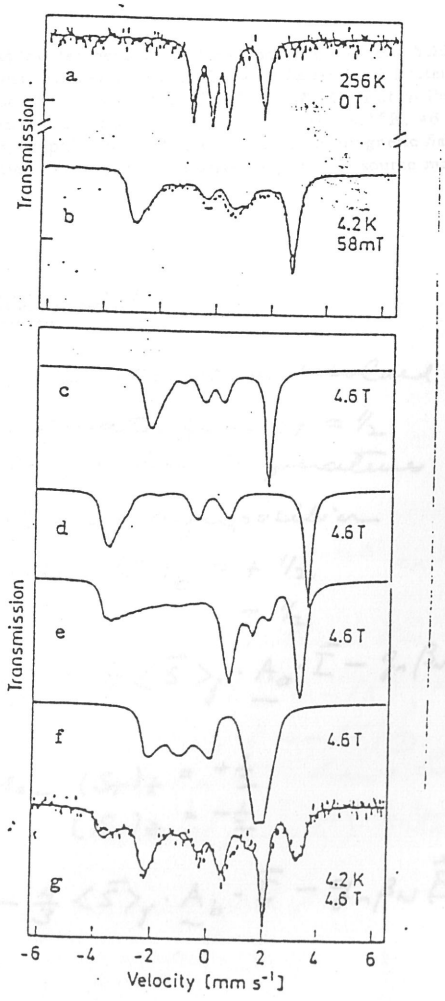

2 quadrupole doublets (1:1) at 0T

Site 1: $\delta(\alpha\text{-Fe}) = 0,29$ mm/s
$\Delta E_Q = 0.64$ mm/s
∴ high-spin Fe^{3+}

Site 2: $\delta(\alpha\text{-Fe}) = 0,56$ mm/s
$\Delta E_Q = 2.63$ mm/s
∴ high-spin Fe^{2+}

both tetracoordinated to sulfur ligands

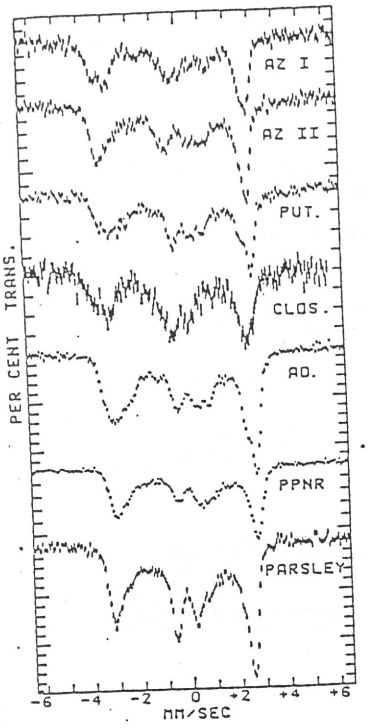

Mössbauer spectra at low temperature and small applied magnetic field for reduced plant-type ferredoxins. Abbreviations: AZI = *Azotobacter* Fe-S Protein I, 4.2 °K, 1.15 kG; AZII = *Azotobacter* Fe-S Protein II, 4.2 °K, 300 G; Put. = Putidaredoxin, 4.6 °K, 580 G; Clos. = Clostridial Paramagnetic Protein, 4.7 °K, 3.4 kG; Ad. = Pig Adrenodoxin, lyophilized, 5.3 °K, 580 G; PPNR = Spinach Ferredoxin, lyophilized, 4.3 °K, 580 G; Parsley = Parsley Ferredoxin, 5.1 °K, 580 G. Applied magnetic field is parallel to gamma-ray direction. Velocities are relative to platinum source matrix

Weak field

magnetic hyperfine interaction

Cluster is therefore paramagnetic

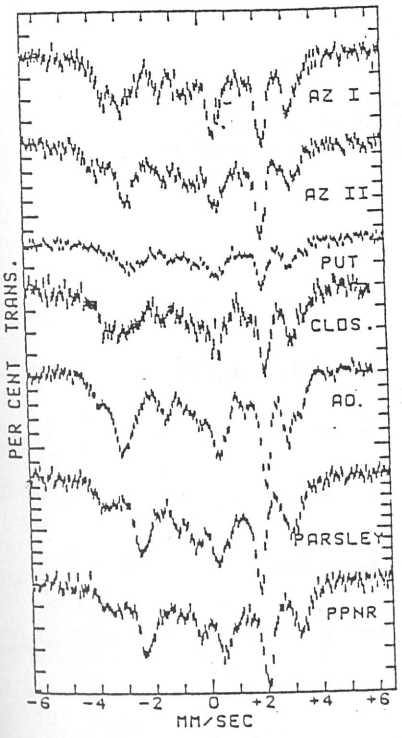

Mössbauer spectra at low temperature and high applied magnetic field for reduced plant-type ferredoxins. Abbreviations: AZI = *Azotobacter* Fe-S Protein I, 4.2 °K, 46 kG; AZII = *Azotobacter* Fe-S Protein II, 4.2 °K, 46 kG; Put. = Putidaredoxin, 4.6 °K, 46 kG; Clos. = Clostridial Paramagnetic Protein, 4.2 °K, 46 kG; PPNR = Spinach Ferredoxin, lyophilized, 4.3 °K, 46 kG. Applied magnetic field is parallel to gamma-ray direction. Velocities are relative to platinum source matrix

High magnetic field

→ nuclear Zeeman interaction resolved.

→ spectrum originates from $S_T = 1/2$ ground state at low temperatures

→ Observed spectrum is a superposition of $^{57}Fe(III)$ when $(S_T)_z = +1/2$
$-1/2$

$$\left(\mathcal{H}_{n,a} = \mathcal{H}_{Q,a} + \frac{7}{3} \langle \vec{S} \rangle_j \cdot \underset{\sim}{A_a} \cdot \vec{I} - g_n \beta_N \vec{B} \cdot \vec{I} \right)$$

and $^{57}Fe(II)$ when $(S_T)_z = +\frac{1}{2}$
$(S_T)_z = -\frac{1}{2}$

$$\left(\mathcal{H}_{n,e} = \mathcal{H}_{Q,e} - \frac{4}{3} \langle \vec{S} \rangle_j \cdot \underset{\sim}{A_b} \cdot \vec{I} - g_n \beta_N \vec{B} \cdot \vec{I} \right)$$

→ Fe_3S_4 and Fe_4S_4 clusters

* Source : bacteria, eukaryotes

frequently 2 clusters per proteins, e.g. Clostridium pasteurianum and Clostridium acidi-urici (molecular mass 6 kD)

* Most interesting cluster of this class is Chromatium HiPIP because it can be oxidized to give a stable oxidized $[Fe_4S_4]^{3+}$

* X-ray structures known for Chromatium HiPIP and Pseudomonas aeruginea (J. Biol. Chem 1977) 252, 7802-7811)

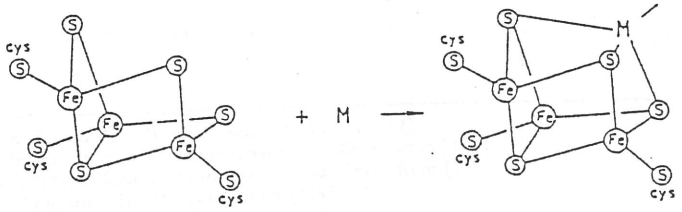

Putative structure of Fe_3S_4 cluster and illustration of conversion into MFe_3S_4 by substituting M = Fe, Co, Zn. EXAFS data of the Fe_3S_4 cluster suggest a compact core with an Fe-Fe distance of 0.27 nm (Antonio et al. (1982) J. Biol. Chem. 257: 6646), just as observed for Fe_4S_4 cubanes

* Mössbauer shows that reduced Fe_3S_4 cluster and Fe_4S_4 cubanes (in all 3 accessible oxidation states) contain a delocalized mixed-valence dimer $Fe\,S_2$.

The delocalized-mixed valence dimer $Fe^{2.5} - Fe^{2.5}$ exhibits isomer shifts just in-between the values characteristic for $Fe^{3+}S_4$ (~ 0.3 mm/s) and $Fe^{2+}S_4$ (~ 0.6 mm/s), and ΔE_Q for $Fe^{3+}S_4$ (~ 0.5 mm/s) and $Fe^{2+}S_4$ (~ 1.8 mm/s)⊙

* The three Fe sites of Fe_3S_4 core in ferredoxin II have been studied under conditions where the fourth (empty) site is occupied by Fe^{2+}, Co^{2+}, or Zn^{2+}. The delocalized pair is

essentially unaltered in the series $[Fe_3S_4]$, $[Fe_4S_4]$, (8)

$[CoFe_3S_4]^{2+}$.

Isomer shifts δ(α-Fe) and quadrupole splittings ΔE_Q of three-iron and four-iron clusters in various oxidation states

cluster	valence		δ (mms^{-1})	ΔE_Q (mms^{-1})	Fe sites	cluster spin
$[Fe_3S_4]^0$	$Fe^{2.5+}$	$-Fe^{2.5+}$	0.46	1.47	2	S = 2
a	Fe^{3+}		0.32	0.52	1	
$[Fe_4S_4]^{1+}$	$Fe^{2.5+}$	$-Fe^{2.5+}$	0.50	1.18	2	S = 1/2
b	Fe^{2+}	$-Fe^{2+}$	0.60	1.82	2	
$[Fe_4S_4]^{2+}$	$Fe^{2.5+}$	$-Fe^{2.5+}$	0.42	1.08	2	S = 0
c	$Fe^{2.5+}$	$-Fe^{2.5+}$	0.42	1.08	2	
$[Fe_4S_4]^{2+}$	$Fe^{2.5+}$	$-Fe^{2.5+}$	0.43	1.14	2	S = 0
d	$Fe^{2.5+}$	$-Fe^{2.5+}$	0.43	1.14	2	
$[Fe_4S_4]^{3+}$	$Fe^{2.5+}$	$-Fe^{2.5+}$	0.40	1.03	2	S = 1/2
e	Fe^{3+}	$-Fe^{3+}$	0.29	0.88	2	
$[Fe_4S_4]^{1+}$	$Fe^{2.5+}$	$-Fe^{2.5+}$	0.51	1.07	2	S = 1/2
f	Fe^{2+}	$-Fe^{2+}$	0.60	1.67	2	
$[Fe_4S_4]^{2+}$	$Fe^{2.5+}$	$-Fe^{2.5+}$	0.45	1.32	2	S = 0
f	$Fe^{2.5+}$	$-Fe^{2.5+}$	0.45	1.32	1	
			0.41	0.55	1	
$[ZnFe_3S_4]^{1+}$	$Fe^{2.5+}$	$-Fe^{2.5+}$	0.52	1.5	1	S = 5/2
				1.7	1	
f	Fe^{2+}	$-Zn^{2+}$	0.62	2.7	1	
$[CoFe_3S_4]^{1+}$	$Fe^{2.5+}$	$-Fe^{2.5+}$	0.53	1.28	2	S > 0
f	Fe^{2+}	$-Co^{2+}$	0.53	1.28	1	
$[CoFe_3S_4]^{2+}$	$Fe^{2.5+}$	$-Fe^{2.5+}$	0.44	1.35	2	S = 1/2
f	Fe^{3+}	$-Co^{2+}$	0.35	1.1	1	

[a] Ferredoxin II from *Desulfovibrio gigas*. Taken from [112].
[b] Reduced ferredoxin from *B. stearothermophilus*. Taken from [113].
[c] Oxidized ferredoxin from *B. stearothermophilus*. Taken from [113].
[d] Reduced *Chromatium* HiPIP. Taken from [114].
[e] Oxidized *Chromatium* HiPIP. Taken from [114].
[f] $[MFe_3S_4]^{1+,2+}$ clusters obtained by incubating ferredoxin II from *Desulfovibrio gigas* in the presence of excess $M = Fe^{2+}, Co^{2+}, Zn^{2+}$. Taken from [115–118].

1e⁻-reduced

3e⁻-reduced →

2e⁻-reduced →

2e⁻-reduced →

1e⁻-reduced →

3e⁻-reduced →

2e⁻-reduced →

2e⁻-reduced →

2e⁻-reduced →

1e⁻-reduced →

The Fe site in $[CoFe_3S_4]^{1+}$ and $[ZnFe_3S_4]^{1+}$ which do not belong to the delocalized pair are formally Fe^{2+}, but the addition of Fe^{3+} to $[Fe_3S_4]^0$, which generates $[Fe_4S_4]^{3+}$, leads to facile 1e⁻ reduction to $[Fe_4S_4]^{2+}$ to give a second delocalized mixed valence Fe_2S_2 because of high reduction potential $[Fe_4S_4]^{3+}$.

In the mixed-valence delocalized Fe_2S_2 units,
δ(α-Fe) vary from 0.40 – 0.53 mm/s
" " 1 – 1.7 mm/s.
ΔE_Q " "

* The two irons in a delocalized mixed valence $Fe^{2.5+} - Fe^{2.5+}$ pair are ferromagnetic exchange coupled to give $S_{pair} = \frac{9}{2}$ and

are not distinguishable. Both Fe sites exhibit the same identical nuclear magnetic hyperfine interaction, for example.

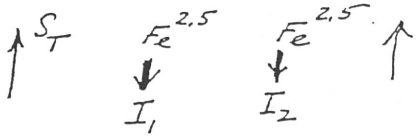

However, these sites can be distinguished from $Fe^{3+/2+}$ sites outside the pair, even though there is also antiferromagnetic exchange interaction between the delocalized mixed valence pair and the $Fe^{3+/2+}$ sites outside the pair. This antiferromagnetic exchange interaction has important consequences on the magnetic hyperfine interaction of the $Fe^{3+/2+}$ outside the pair.

Thus in $[Fe_3S_4]^0$ clusters, the magnetic hyperfine interaction for the Fe^{3+} has a positive sign (usually negative due to Fermi-contact interaction). Reason

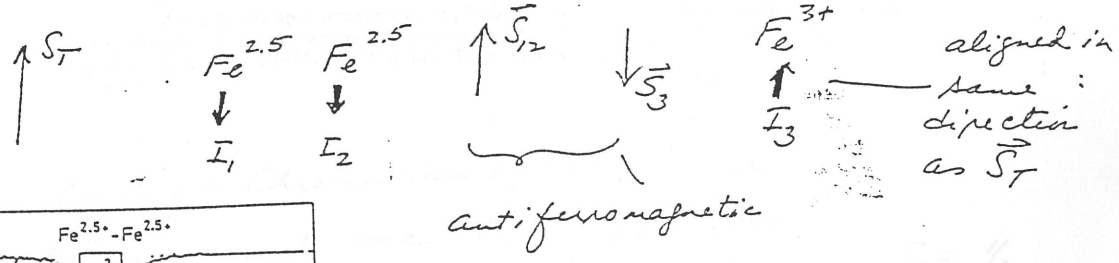

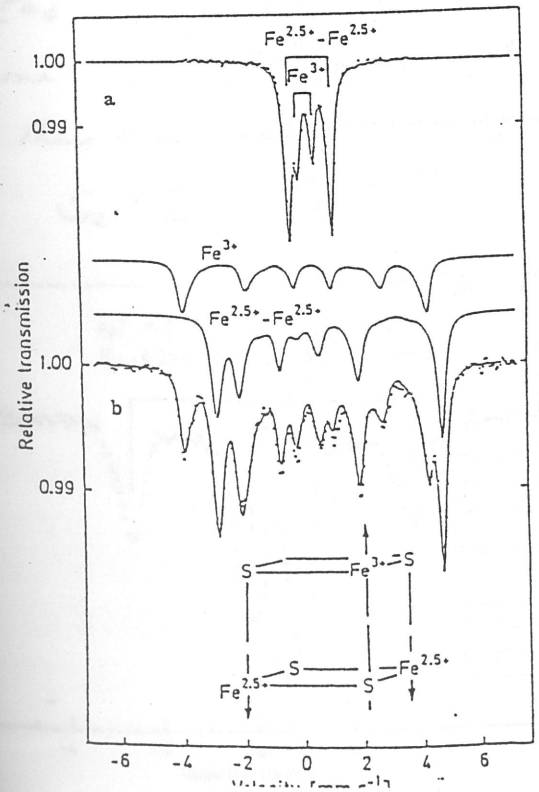

Mössbauer spectra of the reduced Fe_3S_4 cluster of ferredoxin II recorded at 4.2 K in zero field (a) and at 1.3 K in parallel applied field of 1 T (b). The solid lines in (b) are theoretical curves for the delocalized pair and the Fe^{3+} site. The sum is drawn through the experimental data. Taken from [118]. The insert gives a scheme of the proposed spin-coupling: $S = S_{12} + S_3 = 9/2 - 5/2 = 2$

Effective magnetic hyperfine coupling tensors[a] $\bar{A}'_{12}/g_n\beta_n$ and $\bar{A}'_3/g_n\beta_n$ of reduced ferredoxin II [118]

site	$A'_x(T)$ / $g_n\beta_n$	$A'_y(T)$ / $g_n\beta_n$	$A'_z(T)$ / $g_n\beta_n$	$A'_{av}(T)$ / $g_n\beta_n$
$Fe^{2.5+} - Fe^{2.5+}$	−14.9	−14.9	−11.6	−13.8
Fe^{3+}	9.9	11.6	12.6	11.3

[a] Effective tensors $\bar{A}'$ are related to local tensors $\bar{A}$ by $\bar{A}'\langle\vec{S}_i\rangle/g_n\beta_n = \bar{A}\langle\vec{S}_{local}\rangle/g_n\beta_n$

In $[Fe_4S_4]^{2+}$, there are <u>two</u> delocalized valence fragments, each with $S_{12} = S_{34} = 9/2$, and these are antiferromagnetically exchange coupled to give $S_T = 0$. Mössbauer for this cluster exhibit same magnetic hyperfine interaction as $[Fe_2S_2]^{2+}$ ferredoxins, except that ΔE_Q & δ are characteristic of $Fe^{2.5} \cdots Fe^{2.5}$. $2J$ between S_{12} & S_{34} is $-460\ cm^{-1}$.

In $[Fe_4S_4]^{1+}$, there is one delocalized mixed valence pair, and one $Fe^{2+} \cdots Fe^{2+}$ fragment, and these are antiferromagnetically coupled to give $S_T = 1/2$

$$S_{12} = \frac{9}{2}, \quad S_{34} = 4$$

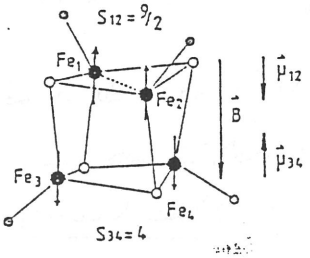

Model for the spin arrangement in $[Fe_4S_4]^{1+}$ in an applied field $\vec{B}$. The *dashed line* indicates the delocalized electron within the $Fe^{2.5+}$–$Fe^{2.5+}$ dimer. Total spin is $S_t = 1/2$

In $[Fe_4S_4]^{3+}$, (oxidized Chromatium HiPIP), there is one $Fe^{2.5} \cdots Fe^{2.5}$ pair and one $Fe^{3+} \cdots Fe^{3+}$ pair and these are antiferromagnetically coupled to give $S_T = 1/2$

$$S_{12} = \frac{9}{2}, \quad S_{34} = 5 \qquad S_T = 5 - 9/2 = 1/2$$

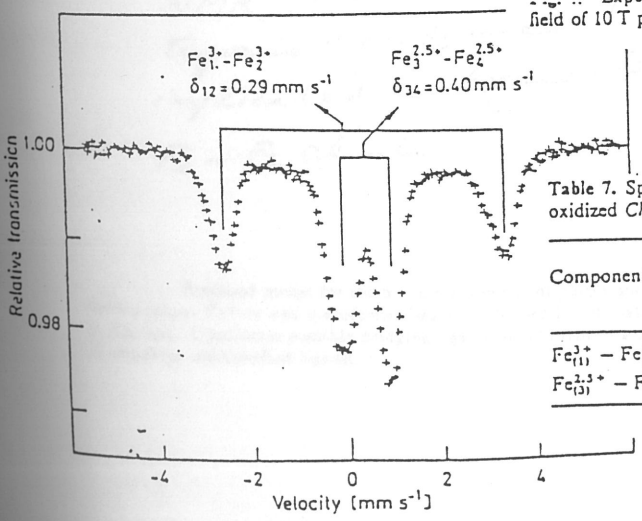

Experimental Mössbauer spectrum of oxidized *Chromatium* HiPIP at 4.2 K in an applied field of 10 T parallel to the γ-beam. Taken from [129]

Table 7. Spin-Hamiltonian parameters obtained from simulating Mössbauer spectra at 4.2 K of oxidized *Chromatium* HiPIP. Taken from [129]

Component	δ(α-Fe) (mms^{-1})	ΔE_Q (mms^{-1})	η	$A'_x(T)/g_n\beta_n$	$A'_y(T)/g_n\beta_n$	$A'_z(T)/g_n\beta_n$
$Fe^{3+}_{(1)} - Fe^{3+}_{(2)}$	0.29	0.88	0.4	+13.9	+16.3	+14.0
$Fe^{2.5+}_{(3)} - Fe^{2.5+}_{(4)}$	0.40	1.03	0.9	−20.5	−22.2	−23.6

* Non-heme iron-oxo proteins (continued)

→ Purple acid phosphatase

* Sources : bovine spleen, rat spleen, human spleen, porcine uterine fluid (uteroferrin); also plants & microbial

* Function : catalyzes phosphate ester, thereby regulating the physiological level of inorganic phosphate and phosphorylated metabolites under acidic conditions

* Molecular mass molecular mass 35-40 kD

* Color : purple/pink chromophore in contrast with the greenish color of met Hr & ribonucleotide reductase. Visible absorption at 510-550 nm ($\epsilon \sim 4000\ M^{-1}\ cm^{-1}$). Raman studies indicate that absorption arises from tyrosinate-to-iron(III) charge transfer.

* EPR and magnetic susceptibility studies indicate that the oxidized (purple) enzyme contains an antiferromagnetically coupled $(Fe^{III})_2$ unit, and the enzymatically active, reduced (pink) enzyme contains a spin-coupled (weak) mixed valence Fe(III) - Fe(II) cluster, for both the bovine spleen & [uterine/porcine] enzymes. (EPR and $g_{av} = 1.7-1.8$ & similar to Hr

* On basis of paramagnetic NMR, both histidine and tyrosine ligands are implicated as ligands to Fe-Fe cluster

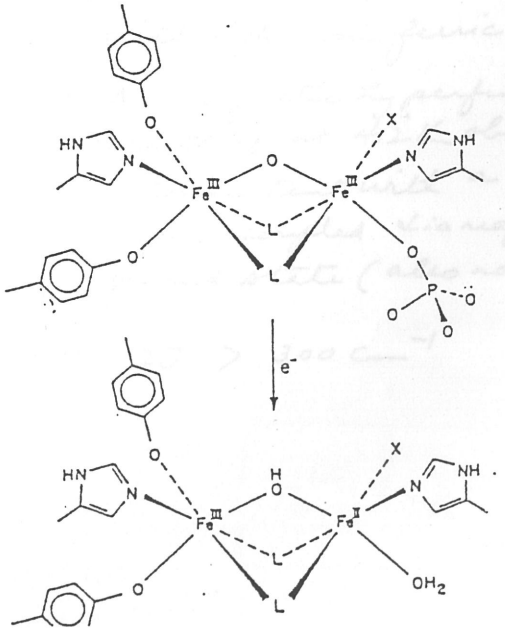

Proposed model for the binuclear iron site of purple and pink bovine spleen FePase and uteroferrin, based on this work and that cited in the text. L indicates possible bridging ligands in addition to a μ-oxo; X indicates unidentified ligand.

* The effect of electron reduction on the absorption, specifically the persistence of the charge transfer transition in the reduced form with almost identical extinction coefficient strongly suggests that tyrosine is coordinated solely to the iron center that remains ferric following reduction. This conclusion is confirmed by resonance Raman studies.

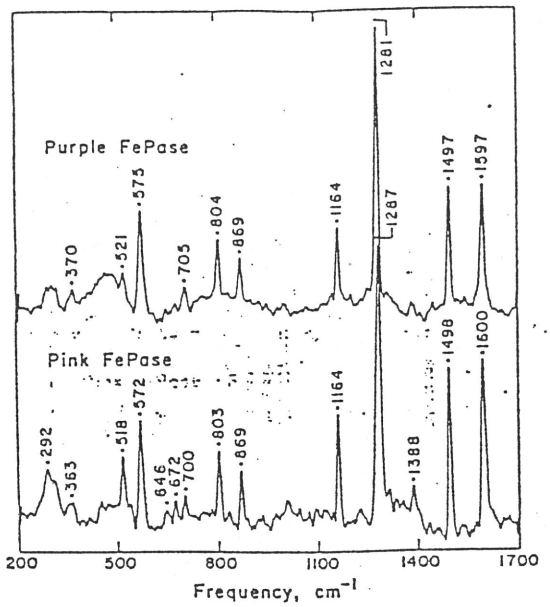

Resonance Raman spectra of 5 mM purple (top) and 2.7 mM pink (bottom) forms of bovine spleen FePase in 10 mM NaOAc buffer, pH 5.0 at 5 °C. Sample temperature was maintained by placing the capillary in the cold-finger of an ice-filled Dewar.[25] Data were collected with use of 514.5-nm excitation, 100-mW incident power, and 140° back-scattering geometry. The spectra shown are an average of 3 scans (purple) and 8 scans (pink) taken at a scan rate of 1 cm^{-1}/s and a slit width of 4–5 cm^{-1} and then subjected to a 13-point smooth.

essentially identical

* Mössbauer spectrum of oxidized bovine spleen FePase

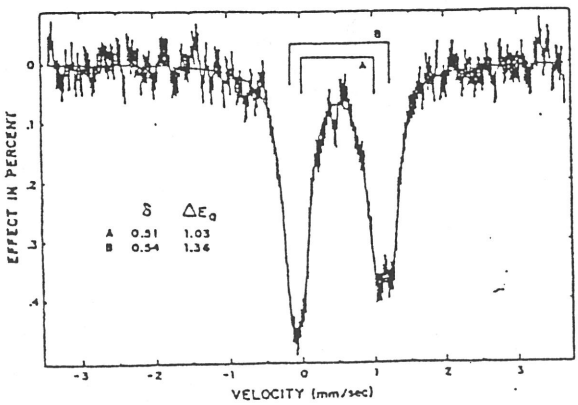

^{57}Fe Mössbauer spectrum at 4.2 K of purple (oxidized) bovine spleen FePase (2 mM in 50 mM NaOAc, pH 5.0). The solid line is a fit to the data with use of the parameters in Table II. Data aquisition time was 47 h.

→ δ and ΔE_Q consistent with high-spin ferric.

→ No magnetic hyperfine splitting at 4.2 K observed — consistent with a spin-coupled diamagnetic ground state (also no EPR).

→ $-2J > 300\ cm^{-1}$

* Oxyanions affect the coordination chemistry of the cluster. Molybdate (MoO_4^{2-}) and tungstate (WO_4^{2-}) are tightly bound noncompetitive inhibitors ($K_I \cong 4 \times 10^{-6}$ M) and phosphate ($H_2PO_4^-$) and arsenate ($H_2AsO_4^-$) are competitive inhibitors ($K_I \sim 1-10$ mM).

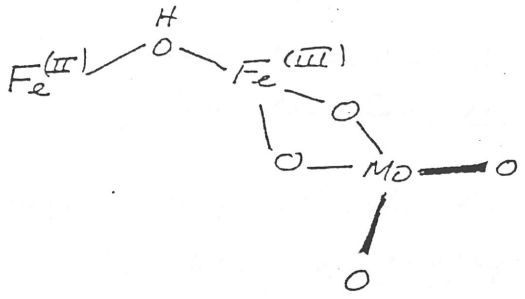

noncompetitive

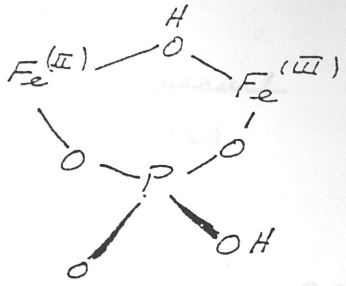

competitive

* Proposed mechanism of phosphate ester hydrolysis

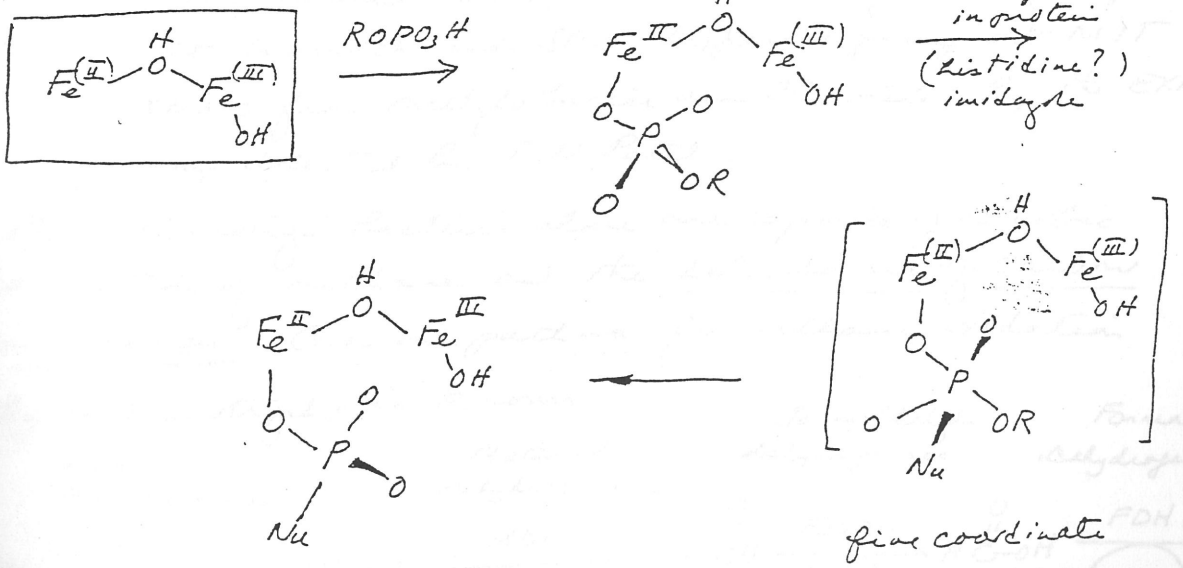

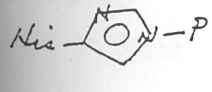

?

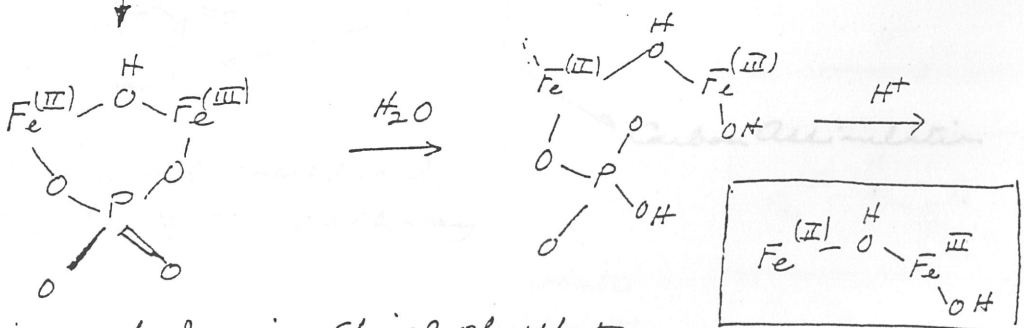

mechanism is being probed using chiral phosphates to ascertain whether the configuration of P is retained or

→ Soluble Methane Monooxygenase (sMMO)

Ref. Brian G. Fox, W. A. Froland, J. E. Dege and John D. Lipscomb
J. Biol. Chem. 264, 10023-10033 (1989)

Brian Fox, Y. Liu, J. E. Dege and J. D. Lipscomb
J. Biol. Chem. 266, 540-550 (1991)

M. P. Hendrich, B. G. Fox, K. K. Andersson, P. G. Debrunner, and J. D. Lipscomb
J. Biol. Chem. 267, 261-269 (1992)

M. P. Hendrich, E. Münck, B. G. Fox, J. D. Lipscomb
J. Am. Chem. Soc. 112, 5861-5865 (1992)

* Source: Methanotrophic bacteria

The sMMO from Methylosinus trichosporium OB3b is the best characterized (Minnesota group headed by Dr. John Lipscomb)

sMMO from Methylococcus capsulatus Bath is being studied also by Howard Dalton and his group at Warwick and Steve Lippard's group at MIT

sMMO from methylobacterium CRL-26 by the EXXON group directed by R. N. Patel.

The methanotropic bacteria alone are capable of aerobic oxidation of methane as the sole source of carbon and energy. One one pathway for methane oxidation by methanotrophs is known.

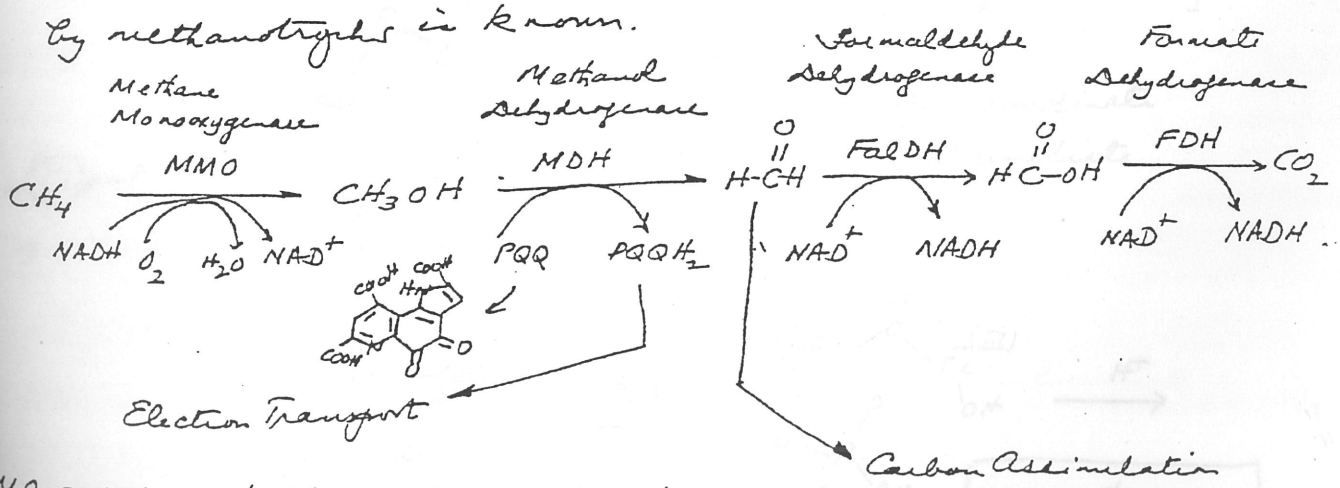

MMO catalyzes the first and energetically most difficult step of this pathway

* Oxyanions affect the coordination chemistry of the cluster. Molybdate (MoO_4^{2-}) and tungstate (WO_4^{2-}) are tightly bound noncompetitive inhibitors ($K_I \cong 4 \times 10^{-6}$ M) and phosphate ($H_2PO_4^-$) and arsenate ($H_2AsO_4^-$) are competitive inhibitors ($K_I \sim 1-10$ mM).

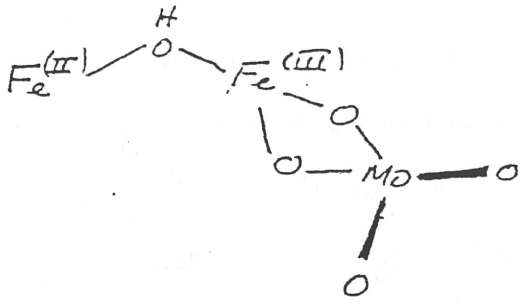

noncompetitive

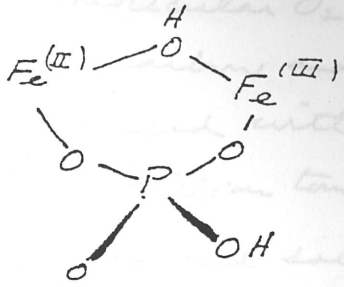

competitive

* Proposed mechanism of phosphate ester hydrolysis

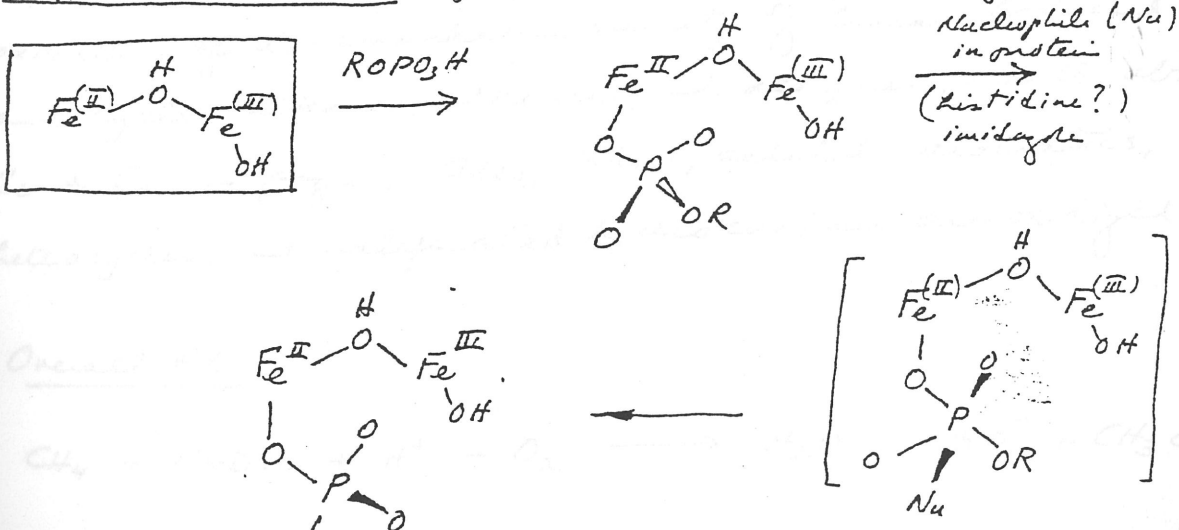

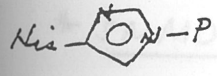

?

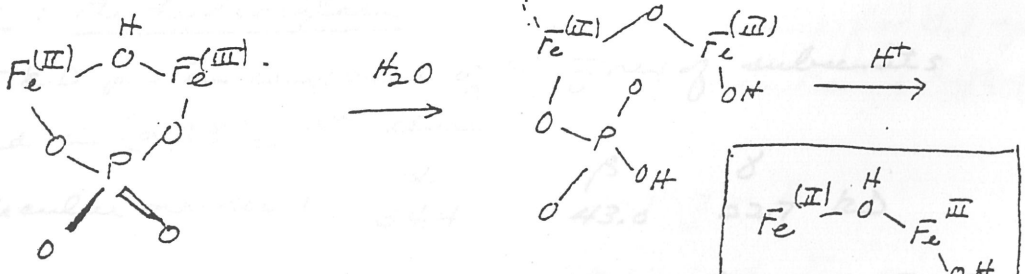

mechanism is being probed using chiral phosphates to ascertain whether the configuration of P is retained or inverted following hydrolysis.

* Significance

Methanotrophic bacteria occupy an environmental niche at the interface of the anaerobic and aerobic environment of our planet. These bacteria intercept the CH_4 produced as the major product of anaerobic metabolism and oxidize it to CO_2 at the expense of molecular O_2. Methane serves as the sole source of carbon and energy of these organisms. It is scavenged with such efficiency that less than 5% of the ~1 billion tons of CH_4 generated in aquatic environments and soils annually escapes into the atmosphere. Note that CH_4 is a potent greenhouse gas (~20 times that of CO_2). Bacteria possessing MMO also catalyze the fortuitous oxidation of a remarkable variety of linear, branched and cyclic alkanes, alkenes, and alkynes, up to about C_6 or C_8 in size. Also, ethers, alcohols, aromatics, heterocycles, and halogenated hydrocarbons are oxidized.

* Overall RX

$$CH_4 + NADH + H^+ + O_2 \longrightarrow H_2O + NAD^+ + CH_3OH$$

$$\Delta G^{0\prime} = -40.6 \text{ kJ/mole}$$

* SMMO

a protein complex with 3 components:

(1) Protein A : the hydroxylase

(a) a 245 kD protein composed of 3 types of subunits arranged in $(\alpha\beta\gamma)_2$ structure

(b) molecular masses: α 54.4, β 43.0, γ 22.7 kD

(c) 4 mol Fe / mol protein (2 non-heme iron oxo Fe-Fe clusters)

(d) no acid labile S^{2-} and no heme

(e) site of hydroxylase activity or monooxygenase activity.
(f) crystals diffract to ~2Å (D. Ohlendorf)

(2) Protein C : the reductase

(a) a 40 kD monomeric protein containing FAD and a [2Fe-2S] cluster.

(b) functions as an NADH oxidoreductase, transferring reducing equivalents from NADH to the hydroxylase

(c) small crystals available

(3) Protein B : the regulatory component

(a) contains no metals or cofactors

(b) regulates activity of hydroxylase and substrate specificity and stereoselectivity of hydroxylation

(c) molecular mass 15.8 kD

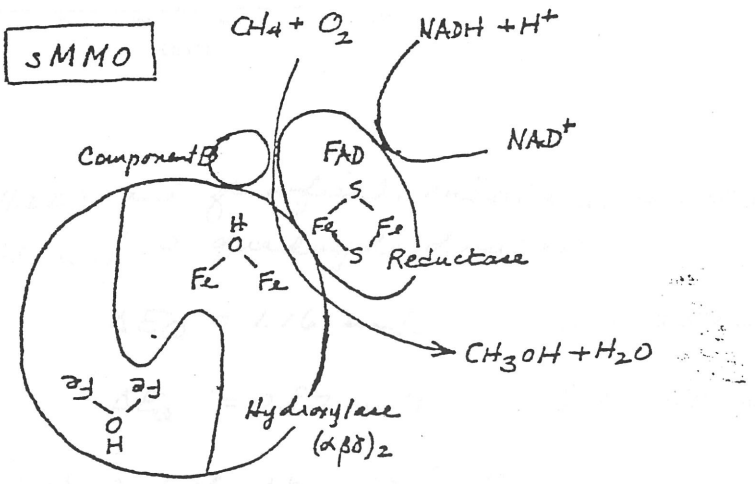

(d) small crystals available; solution structure recently worked out by Lipscomb et al. (19

* The hydroxylase contains two Fe-oxo clusters

(1) Oxidized clusters

(a) Weak EPR at $g = 4.3$ and 2.0 accounting for 0.1 spin per mol due to adventitiously bound Fe^{3+} (high spin ferric in rhombic environment)

(b) an integral spin EPR signal at $g \sim 8$

This signal arises from $S = 2$ multiplet of the antiferromagnetically exchange-coupled $Fe^{3+} \cdots Fe^{3+}$. Analysis of

temperature dependence of this signal yields $-2J = 15\ cm^{-1}$ (weak antiferromagnetic coupling!), more than an order of magnitude smaller than $-2J$ for oxo-bridged Fe clusters of HR and ribonucleotide reductase.

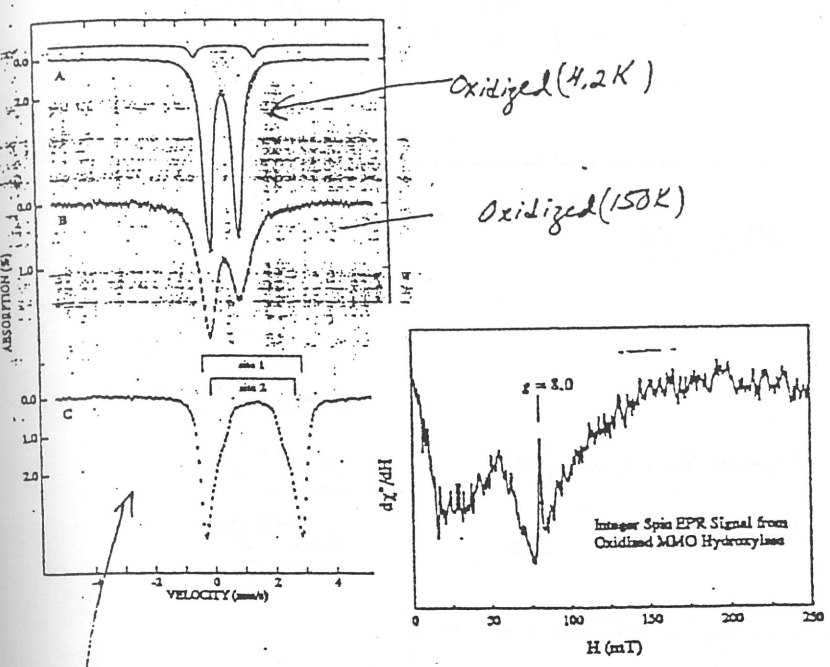

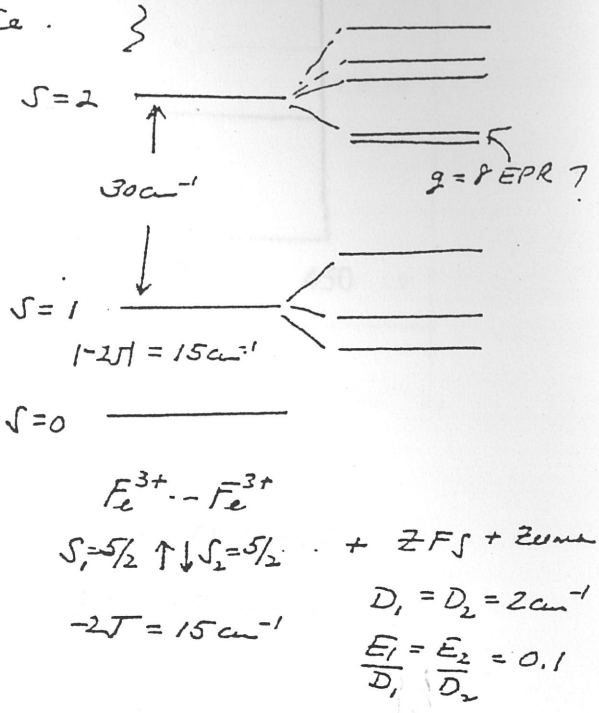

fully reduced 4.2K

(C) Mössbauer

at low temp (4.2K) and zero field, Mössbauer spectrum is a superposition of 2 quadrupole doublets

Site 1 $\quad \Delta E_Q = 1.16$ mm/s $\quad \delta = 0.51$ mm/s

Site 2 $\quad \Delta E_Q = 0.87$ mm/s $\quad \delta = 0.50$ mm/s

Consistent with 2 high-spin Fe^{3+} ion.

(2) Mixed valence $Fe^{2+}Fe^{3+}$ oxo cluster

(a) EPR spectrum is consistent with antiferromagnetically coupled $Fe^{3+}(S = 5/2) \cdots Fe^{2+}(S = 2)$ cluster

effective g values $\quad g_x = 1.77,\ g_y = 1.86\ \ g_z = 1.94$

Fe^{3+} site : $g_{intrinsic}$ assumed isotropic $= 2.00$

Fe^{2+} site : $D = 4.1\ cm^{-1}$, $\quad E/D = 0.34$

$g_x = 2.10$; $g_y = 2.14$; $g_z = 2.045$ intrinsic

$-2J = 60\ cm^{-1}$

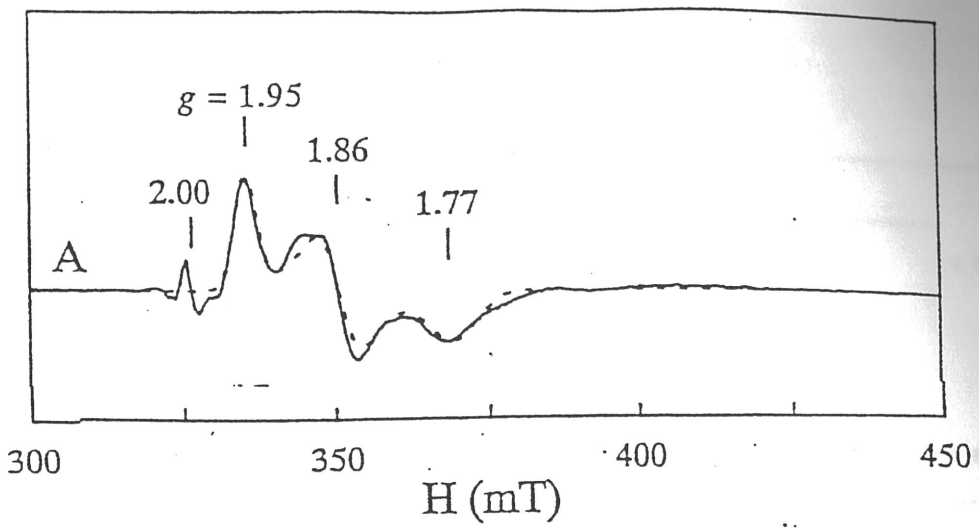

(b) Mössbauer

Fe^{3+} site: $\Delta E_Q = -1.3$ mm/s $\quad \delta = 0.48$ mm/s

Fe^{2+} site $\quad \Delta E_Q = +2.4$ mm/s $\quad \delta = 1.19$ mm/s

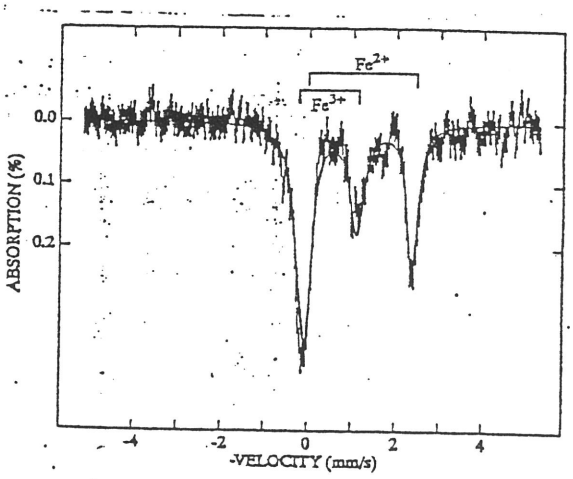

Mixed valence

(c) ENDOR studies revealed coordinating nitrogens to the iron

Based on these results and alignment of the hydroxylase amino acid sequence in the assumed active site region and that of the R2 cluster region in ribonucleotide reductase suggest the ligand structure of the active shown to the right

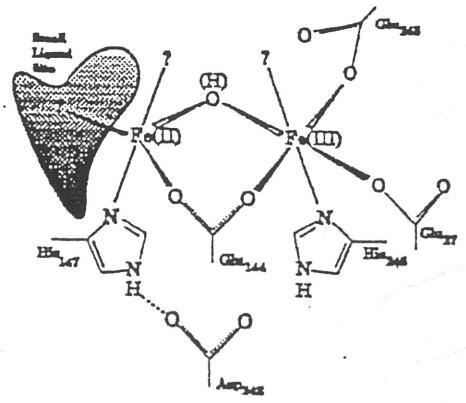

(a) Fully reduced Fe(III) – Fe(II) Cluster

(a) Integer spin EPR signal observed at $g = 16$

EPR spectra (—) and simulations (--) of the fully reduced methane monooxygenase hydroxylase component at 4 K using microwave field B_1 parallel (a) and perpendicular (b) to the static field B. Simulation parameters: $D = 1.2\ cm^{-1}$; $E/D = 0.16$; $\sigma_{E/D} = 0.07$ (1 standard deviation); $g_y = 2.00$ for the ground doublet of an $S = 4$ multiplet. Instrumental parameters: microwave frequency, 9.1 GHz at 2 mW (unsaturated); modulation, 100 kHz at 0.8 mT(pp) gain, 1.25×10^5; dB/dt, scan rate, 1 mT/s; filter, 0.5 s. Protein data: protein concentration, 1 mM after addition of reductants and mediators; specfic activity, 500; 2.3 mol of Fe/mol of protein (~0.9 mM oxidized iron clusters). Mössbauer studies of this sample have been previously reported.

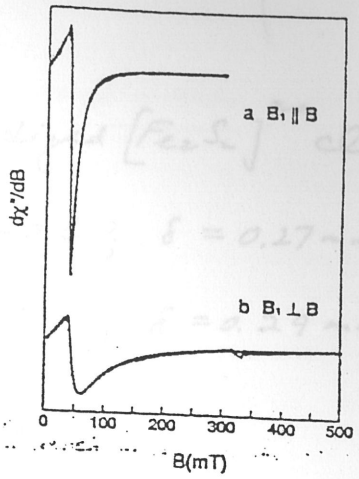

(b) Interpretation of $g = 16$ signal

Weak ferromagnetic coupling between 2 Fe^{2+} ion (high spin)

$S_1 = 2$ $\quad S_2 = 2$

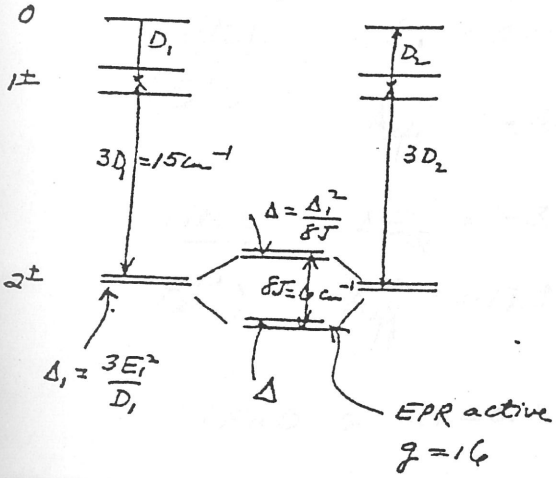

$D_1 = D_2 = -5\ cm^{-1}$

$-2J = -0.75\ cm^{-1}$

$\frac{E_1}{D_1} = 0.27$

(c) Binding of component B (regulatory protein) affects $g = 16$ signal indicating allosteric interaction

Effect of the component B on the *X*-band EPR spectra of the hydroxylase. The hydroxylase (250 μM) was reduced to the fully reduced state as described under "Experimental Procedures." Component B was added anaerobically to give the molar ratios relative to MMOH shown. The MMOH preparation used for this experiment contained at least 1.7 diiron clusters/MMOH molecule; thus a component B to hydroxylase molar ratio of 2.0 is equivalent to about one component B/hydroxylase active site. *Inset:* ●, percent of complete change in EPR line shape determined from the spectra of the fully reduced hydroxylase shown in the main figure (see "Experimental Procedures") as a function of the component B to hydroxylase molar ratio; □, equivalent data for the titration of the mixed valent hydroxylase with component B presented for comparison (Fig. 4 from Ref. 10). Instrumental conditions: gain, 2000; scan range; 200 millitesla; scan center, 100 millitesla; modulation amplitude, 1 millitesla; modulation frequency, 100 kHz; microwave frequency, 9.23 GHz; microwave power, 1.0 milliwatts; temperature, 10.0 K.

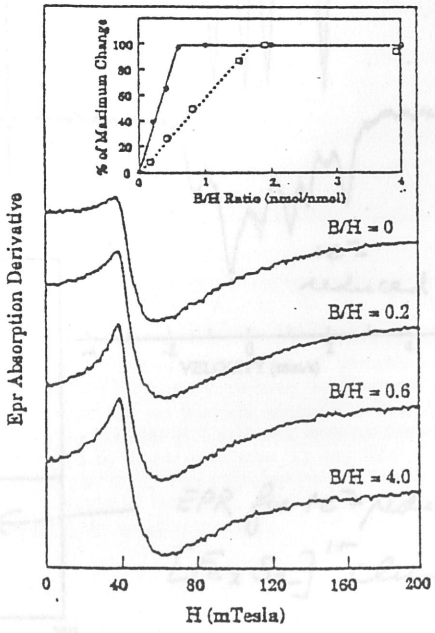

* Protein C, the reductase

(1) 1 flavin adenine dinucleotide (FAD)

1 Fe_2S_2 cluster

(2) ^{57}Fe Mössbauer spectrum of oxidized $[Fe_2S_2]^{2+}$ cluster

site 1 : $\Delta E_Q = 0.50$ mm/s ; $\eta = 0.6$; $\delta = 0.27$ mm/s

site 2 : $\Delta E_Q = 0.80$ mm/s ; $\eta = 1.0$; $\delta = 0.29$ mm/s

Expected for two high-spin ferric ions

(3) ^{57}Fe Mössbauer spectrum of reduced $[Fe_2S_2]^{1+}$ cluster

site 1 : $\Delta E_Q = 0.59$ mm/s ; $\eta = 0$; $\delta = 0.31$ mm/s

(Fe^{3+}) $A_{eff}^x = -53.5$ MHz ; $A_{eff}^y = -46.8$ MHz ; $A_{eff}^z = -43.0$ MHz

site 2 : $\Delta E_Q = -3.00$ mm/s ; $\eta = 0.86$; $\delta = 0.65$ mm/s

Fe^{2+}) $A_{eff}^x = +13.8$ MHz ; $A_{eff}^y = +14.8$ MHz ; $A_{eff}^z = +36.5$ MHz

1 FAD & 2.1 ± 0.1 Fe/mole

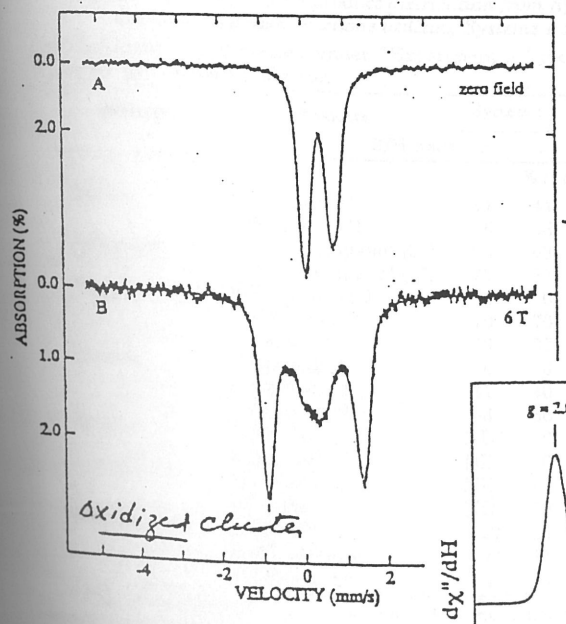

$[Fe_2S_2]^{2+}$

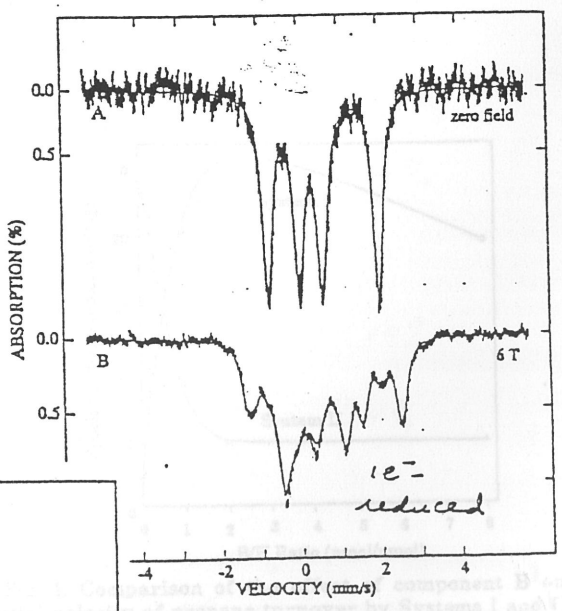

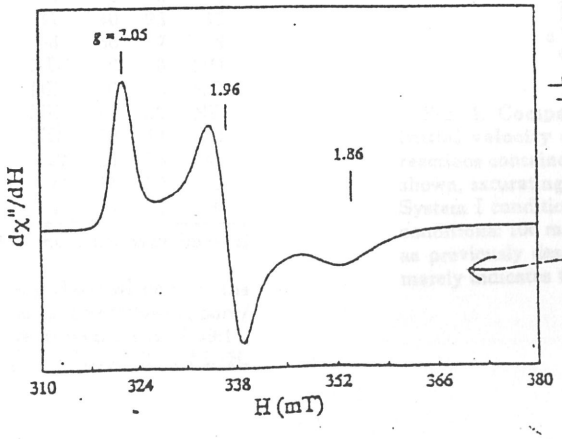

EPR for 1e⁻-reduced $[Fe_2S_2]^{1+}$ cluster

(4) EPR of $[Fe_2S_2]^{1+}$, reduced cluster

effective g value : $g_x = 1.96$; $g_y = 1.86$; $g_z = 2.05$

* Proposed mechanism of methane monooxygenase

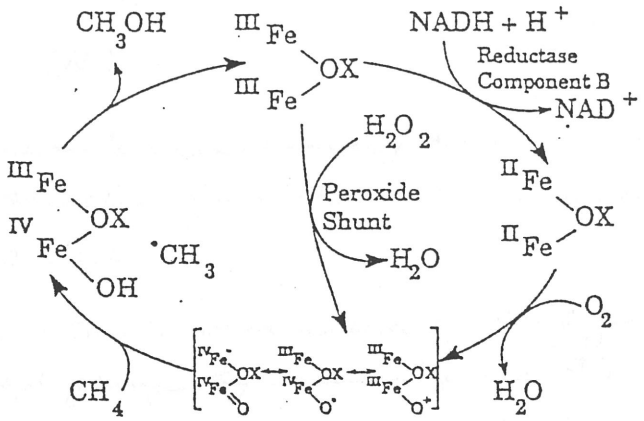

SCHEME 1. Proposed mechanism of methane monooxygenase. $X = H$ or R. The actual point of substrate binding to the enzyme in the cycle unknown.

* Product distribution from hydroxylase catalyzed oxidation reactions vary with B/H [Component B/Hydroxylase] and method of activation of iron-oxo cluster

System I : MMO hydroxylase, NADH, Reductase, O_2

System II : MMO hydroxylase, H_2O_2

Effect of component B on product distribution from hydroxylase catalyzed oxidation reactions utilizing Systems I and II

Conditions are described under "Experimental Procedures." See Table I for evaluation of error.

Substrate	Products	System I		System II	
	B/H Ratio	0	2	0	2
		% of total			
Butane	2-Butanol (2°)	94	44	95	95
	1-Butanol (1°)	6	56	5	5
Isobutane	2-CH_3-2-propanol (3°)	78	63	61	64
	2-CH_3-1-propanol (1°)	22	37	39	36
Pentane	3-Pentanol (2°)	0	0	0	0
	2-Pentanol (2°)	70	70	85	86
	1-Pentanol (1°)	30	30	15	14
Hexane	3-Hexanol (2°)	0	0	0	0
	2-Hexanol (2°)	42	40	93	95
	1-Hexanol (1°)	58	60	7	5
Octane	4-Octanol (2°)	ND[a]	0	0	ND
	3-Octanol (2°)	ND	0	0	ND
	2-Octanol (2°)	ND	82	82	ND
	1-Octanol (1°)	ND	18	18	ND
NO_2-benzene[b]	*p*-NO_2-phenol	<10	89	33	59
	m-NO_2-phenol	>90	11	59	41
	o-NO_2-phenol	0	0	3	0

[a] ND, none detected due to the low yield under the experimental conditions employed.

[b] For this substrate the *ortho* product was observed only in the absence of component B and only for System II. The following *para/meta* product distributions were observed: in System I-1 B/H 89:11, 0.5 B/H 89:11, 0.1 B/H 83:17, in System II-0.5 B/H, 40:60, 1.0 B/H, 48:52.

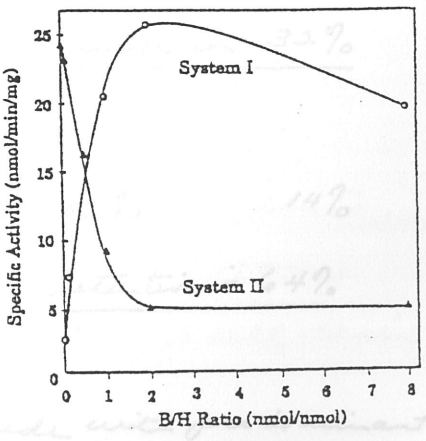

FIG. 1. Comparison of the effect of component B on initial velocity of propane turnover by Systems I and II reactions contained 127 μM MMOH, component B in the mo... shown, saturating propane at 1 atm and were conducted at ... System I conditions: 25 μM reductase, 18 mM NADH. ▲, ... conditions: 100 mM H_2O_2. The *solid line* for the System I ... as previously described (10). The *solid line* for the System II merely indicates the trend of the data.

* An experiment that bears on the mechanism

The steric course of the oxidation of (S)- or (R)- [1-^{2}H, ^{3}H] ethane to ethanol catalyzed by soluble MMO.

(1) Start with 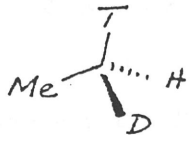 or 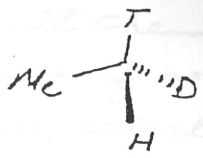

(R) (S)

(2) Exploit the intramolecular primary kinetic isotope effect for hydrogen abstraction from the labeled methyl group of $k_H/k_D = 4.2 \pm 0.2$

(3) Determine the retention or inversion of configuration at the labeled methyl group by examining the ^{3}H NMR of the (2R)-2-acetoxy-2-phenylethanoate derivatives of the ethanol samples

(4) Percentage distribution of ^{3}H label in the methylene group of the (2R)-2-acetoxy-2-phenylethanoate derivatives

Substrate \ Product	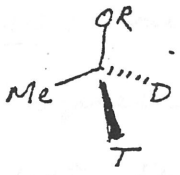	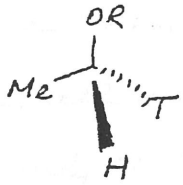	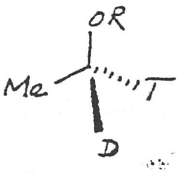	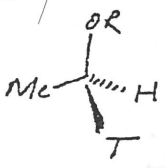
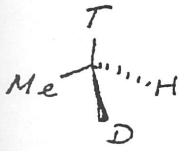 (R)	53%	12%	26%	9%
	retention = 68%		inversion 32%	
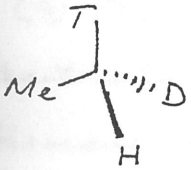 (S)	27%	7%	52%	14%
	inversion = 36%		retention = 64%	

(5) Bottom line: The hydroxylation of ethane proceeds with predominant retention of configuration. However, there is ~ 35% inversion, suggesting that the free substrate intermediate (the radical) is sufficiently long-lived to undergo configuration inversion with appreciable frequency. I can only be ethyl radical because ethyl

• Particulate MMO (The other methane monooxygenase)

→ Alkane activation is a difficult chemical process, often requiring stringent conditions if not expensive and unstable catalysts. However, selective alkane activation and oxidation is achieved in biological systems under ambient conditions, mostly by the particulate MMO. The enzyme methane monooxygenase in methanotrophic bacteria is able to fix CH_4 and oxidize it to CH_3OH using O_2 as a co-substrate.

→ Particulate MMO (pMMO) is a membrane protein, in contrast to sMMO, which is water soluble.

(1) The two forms of MMO differ in their cellular location

sMMO : cytoplasm

pMMO : membrane membrane.

(2) pMMO is expressed in all methanotrophs

(3) sMMO is restricted to only certain strains of methanotroph

Methylococcus capsulatus

Methylosinus trichosporium and

Methylocinus sporium

(4) Expression of sMMO depends on growth conditions, particularly the availability of Cu ions, i.e., the copper to biomass ratio. Under severely-limited copper conditions (no copper added to the growth medium and high cell density), the sMMO is expressed.

→ pMMO and sMMO are distinct enzymes

(1) The two forms of MMO are products of different genes, and hence are structurally distinct proteins.

(2) The gene for the hydroxylase component of sMMO has

been cloned and portions of the sequence have been used to probe cDNA libraries from a variety of methanotrophic bacteria. Hybridization has been observed only with those strains in which sMMO has been previously expressed.

(3) sMMO and pMMO exhibit different substrate specificity

(a) pMMO is primarily specific toward C_1 to C_4.

(b) sMMO is more promiscuous toward substrates.

(c) pMMO is also more sensitive to inhibition by dioxygen "analogs" (N_3^-, CN^-) and metal chelators

The substrate specificity of the soluble methane monooxygenase from *Methylococcus capsulatus* (Bath)

Substituted methane derivatives	*% of rate with methane*	C_1–C_8 *n-alkanes*	*% of rate with methane*	*Products*
Chloromethane	99	Ethane	81	ethanol
Bromomethane	78	Propane	82	propan 1-ol and propan 2-ol
Iodomethane	0	Butane	92	butan 1-ol and butan 2-ol
Dichloromethane	97	Pentane	87	pentan 1-ol and pentan 2-ol; not pentan 3-ol
Trichloromethane	41	Hexane	48	hexan 1-ol and hexan 2-ol; not hexan 3-ol
Tetrachloromethane	0	Heptane	87	heptan 1-ol and heptan 2-ol; not heptan 3-ol or heptan 4-ol
Cyanomethane	39			
Nitromethane	53	Octane	11	octan 1-ol and octan 2-ol; not octan 3-ol or octan 4-ol
Methanethiol	75			
Methanol	239			
Trimethylamine	0			
Carbon monoxide	72			

C_2–C_8 *n-alkanes*	*% of rate with methane*	*Products*	*Alicyclic, aromatic and heterocyclic compounds*	*% of rate with methane*	*Products*
Ethene	176	Epoxyethane	Cyclohexane	74	cyclohexanol
Propene	99	1,2-epoxypropane	Benzene	74	phenol
But-1-ene	58	1,2-epoxybutane	Toluene	63	benzyl alcohol and cresol
cis-But-2-ene	68	*cis*-2,3-epoxybutane and *cis*-buten 1-ol	Styrene	56	styrene epoxide
			Pyridine	35	pyridine N-oxide
trans-But-2-ene	168	*trans*-2,3-epoxybutane and *trans*-2-buten 1-ol	L-Phenylalanine	0	none
Ethers					
Dimethyl ether	295	not known			
Diethyl ether	54	ethanol and ethanal			

(4) $H-C\equiv C-H$ is a suicide substrate for both the sMMO and pMMO. A different polypeptide, of molecular mass 26 kDa in the case of pMMO and 56 kDa in the case of sMMO, is radioactive-labeled when $H-{}^{14}C\equiv C-H$ is employed.

→ Protein Expression

(1) Cu^{2+} induces expression of pMMO and suppresses expression of sMMO.

(2) New polypeptides of apparent molecular masses 46, 35

and 26 kDa appear on protein gels from membranes when cells expressing sMMO are switched over to express pMMO.

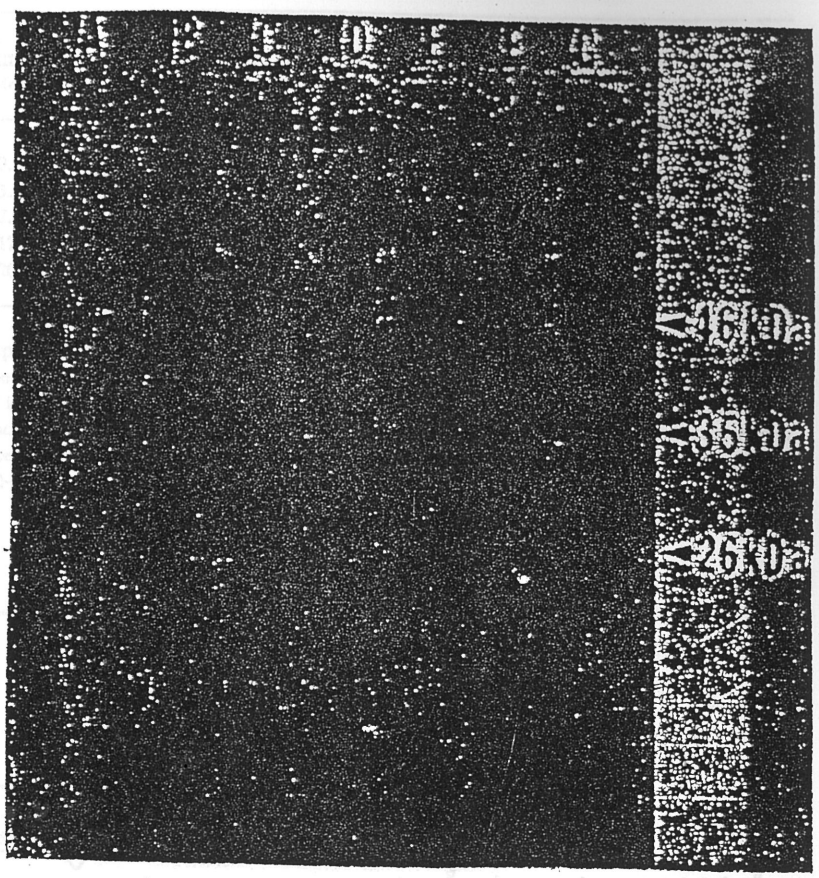

MW standards ⟶ increasing Cu^{2+} concentration

(3) Concomitant with the expression of the pMMO, one observes the formation of membrane stacks arranged as bundles of disc-shaped vesicles inside the cell.

→ Enzyme activity

(1) pMMO activity of Methylococcus capsulatus (Bath) membrane increases as the copper concentration of the growth medium is increased.

(2) The bulk of the copper ions is taken up into the cells, and then found in the membrane fraction of the cell.

(3) Specific activity of membrane fractions isolated from the cells is correlated with the membrane copper / membrane protein ratio.

(4) The addition of copper ions to membrane suspension during

Effect of Growth Medium Copper Concentration on Bacterial Copper Content and pMMO Activity

Cu Concentration[a] of Media (μM)	Total Intracellular[b] Copper (μmole)	Cu Content (μmole)[c] Soluble	Membrane	Cu/Protein (μg/mg)[d] Soluble	Membrane	Specific Activity (nmole/min/mg)[e] As isolated	w/ Copper added
< 0.3	0.7 (~100)	0.17 (25)	0.53 (75)	0.41	1.32	0.68	19.5
2.0	4.4 (~100)	0.48 (11)	3.88 (89)	1.06	7.08	9.6	27.3
5.0	8.7 (87)	0.78 (9)	7.92 (91)	1.55	13.4	17.6	27.7
10.0	13.7 (69)	1.03 (8)	12.7 (92)	2.53	22.2	26.8	30.2
20.0	22.8 (57)	2.0 (9)	20.8 (91)	4.27	37.5	53.7	22.1

[a] Copper concentration of media after supplemental copper was added. The value of 0.3 μM is the upper limit of the copper concentration in the unsupplemented media. [b] The total amount of copper found in the bacteria (whole cells), determined by DCPE. The number in parentheses is the percentage of the total copper available in the media that is ultimately found in the bacteria. [c] The copper content of the soluble and membrane fractions. The number in parenthesis is the portion of total bacteria copper found in each fraction. [d] The copper/protein ratio of the soluble and the membrane fractions. Protein concentration was determined by the Lowry method. [e] The specific activity of the pMMO in the membrane fractions (per mg of total membrane protein) assayed as isolated or with copper added to the assay buffer (150-μM).

activity assays stimulates pMMO activity further

[Propene epoxidation: $CH_3-CH=CH_2 \xrightarrow{pMMO} CH_3-CH(O)-CH_2$]

(5) Soluble fractions from these cell cultures show no propene epoxidation activity, indicating that only the membrane-bound form of the enzyme is being expressed.

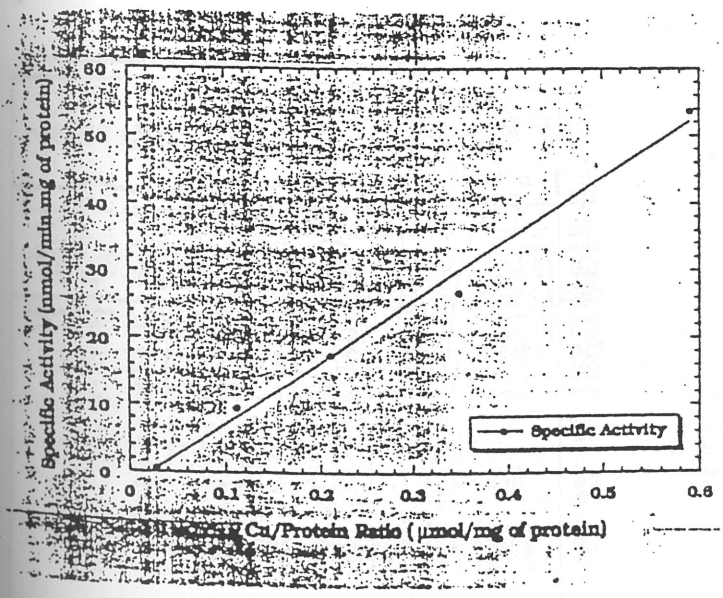

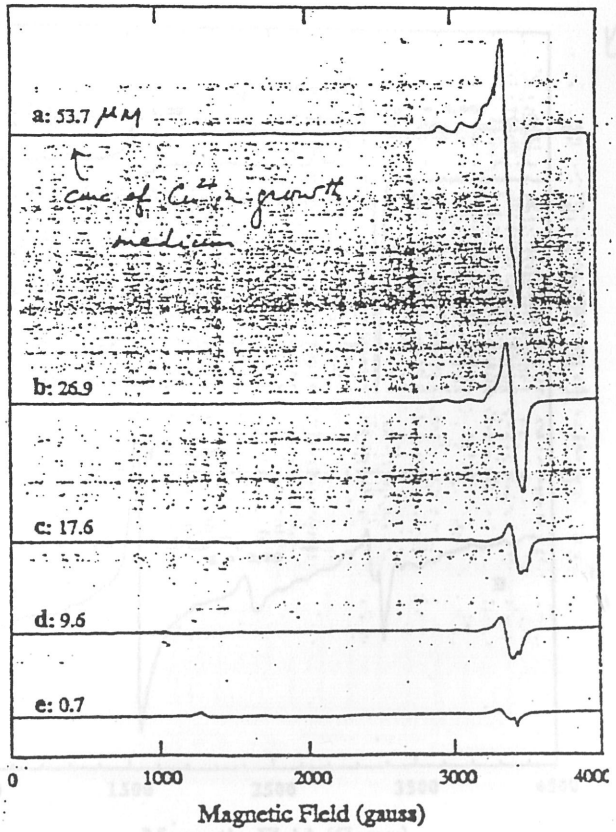

→ Membrane fractions exhibit Cu^{2+} EPR,

(1) Specific activity of membrane fractions correlate with copper EPR intensity However, only ~ 40% of the EPR intensity expected on the basis of

the copper content in the membrane fractions is observed. So part of the Cu^{2+} must be reduced to Cu^{1+}, or they are exchange-coupled to other Cu^{2+} or metal ions, i.e., they exist as part of a cluster.

(2) The membrane fractions exhibit 2 distinct EPR signals (Cu^{2+})

(a) a type 2 copper EPR signal ($g_{\parallel} = 2.25$, $A_{\parallel} \sim 10 \times 10^{-3} cm^{-1}$; $g_{\perp} = 2.058$)

(b) an isotropic EPR signal ($g = 2.06$, broad)

(i) featureless

(ii) difficult to saturate at low temperatures (<10K), and can be isolated by recording the spectrum at high power (Mwave)

With increasing copper in growth medium, intensity of isotropic signal becomes enhanced relative to type 2 copper signal.

(3) Cu EPR is observed in the membrane fractions only when the pMMO is expressed.[A] Membrane suspensions prepared from Methylococcus capsulatus (Bath) cells expressing the sMMO do not exhibit any detectable copper EPR signals

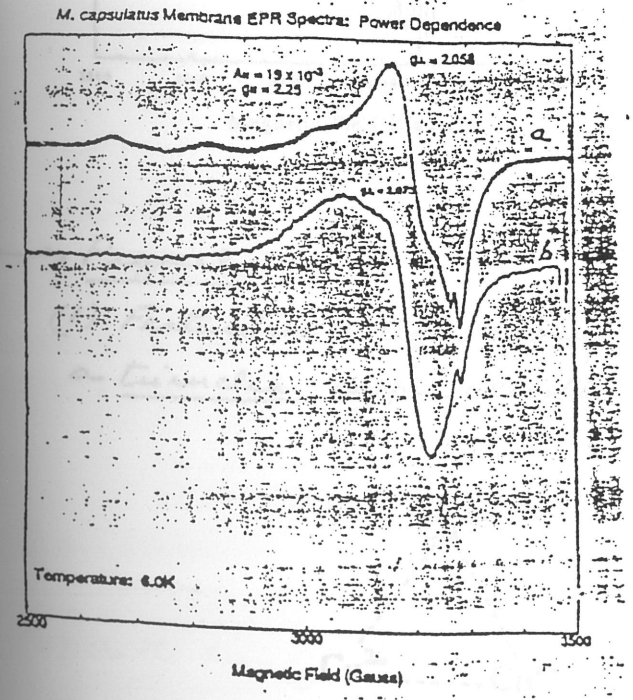

FIGURE 4

Effect of microwave power on the copper EPR spectrum of membranes with active pMMO. The sample contained a suspension of membranes from M. capsulatus grown with 10 μM $CuSO_4$. The spectra were recorded with microwave power of either 0.01 mW (a) or 40 mW (b) at temperature of 6.0 K. This sample exhibited significant pMMO activity.

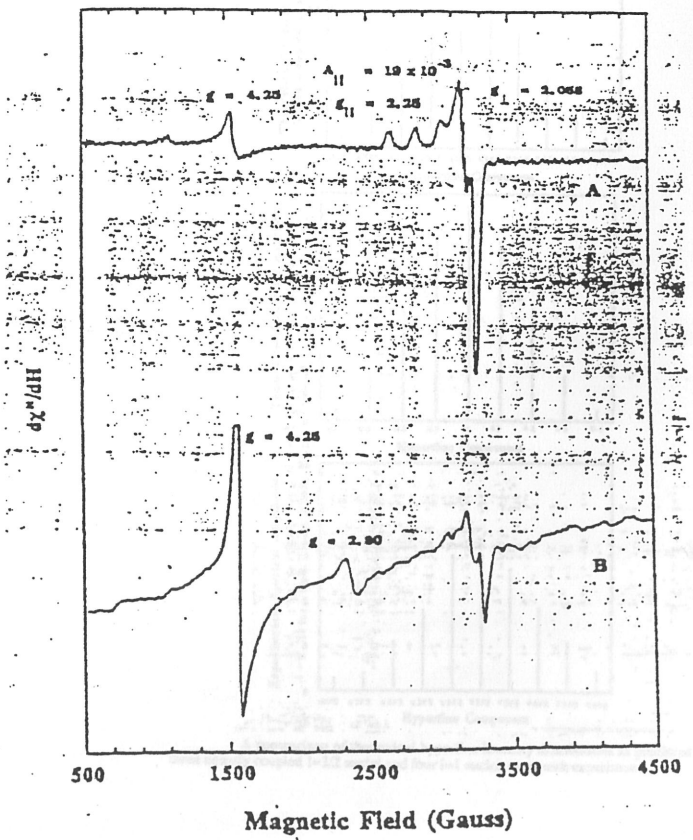

(4) Upon incubation and partial reduction with limiting dithionite, the featureless isotropic signal at g- 2.06 decreases in intensity and gives way to a second isotropic signal at the same g-value but with 10 well-resolved hyperfine components with |A| ~ 15 Gauss. Intensity pattern is consistent with coupling of an electron with 3 equivalent $I = 3/2$ nuclei ($2 \times 3 \times (\frac{3}{2}) + 1 = 10$)

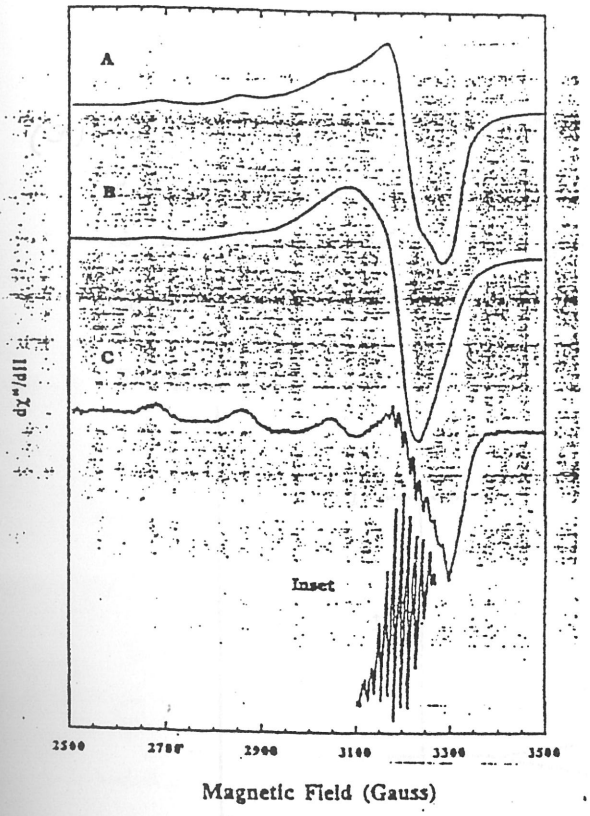

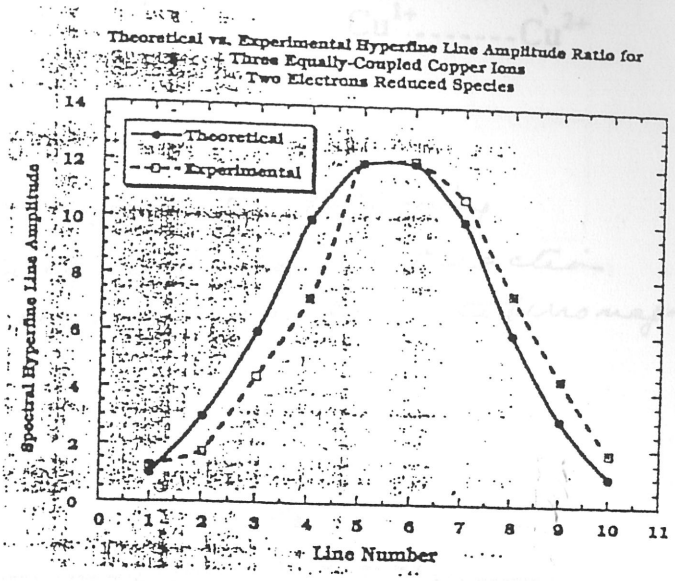

→ Proposal

(1) Featureless isotropic signal is due to a trinuclear copper cluster

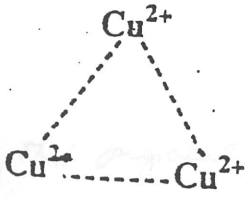

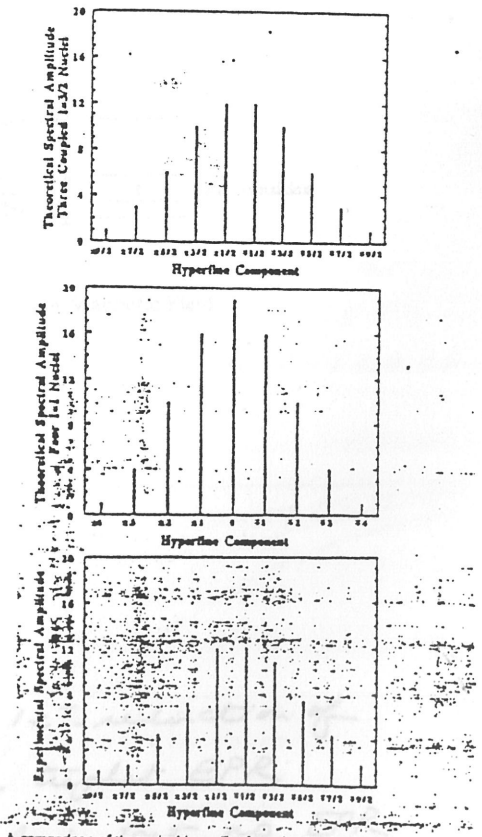

A comparison of theoretical hyperfine intensity distributions as predicted for three equally coupled I=3/2 nuclei and four I=1 nuclei cases with experiment.

(2) $g \sim 2.06$ signal with well-resolved 10-line hyperfine pattern due to partially reduced ($2e^-$) mixed-valence trinuclear copper cluster.

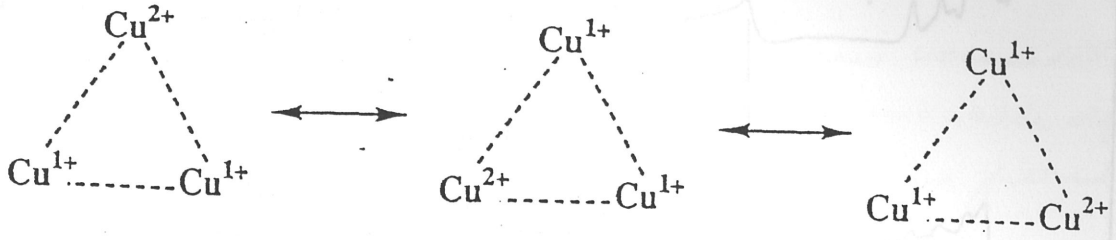

(3) If this proposal is correct, expect the following energy levels for the cluster if the exchange interaction is ferromagnetic (change direction of energy for antiferromagnetic coupling)

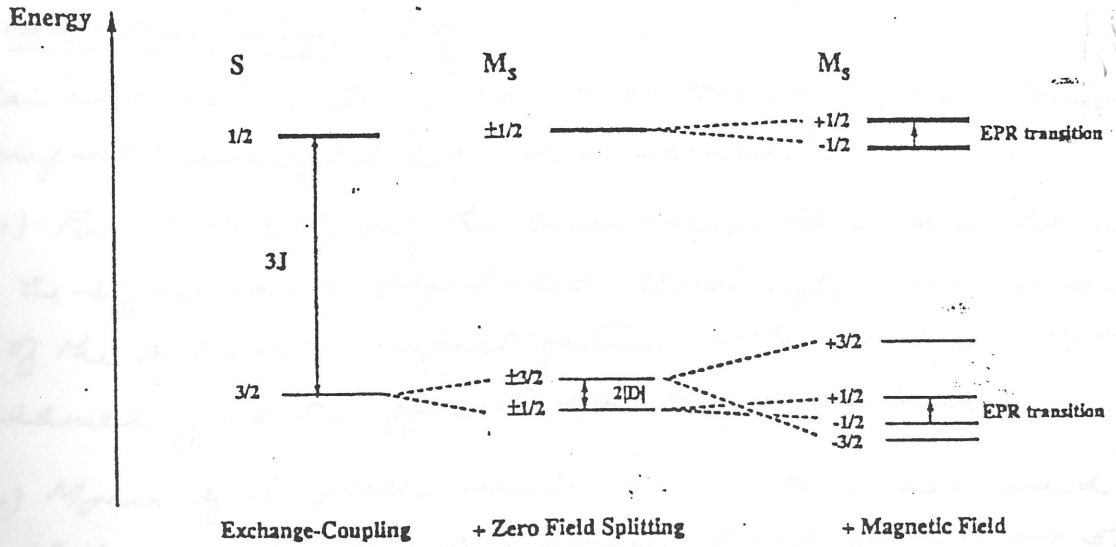

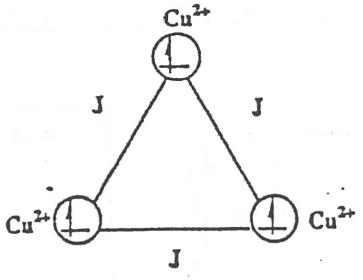

(4) On the basis of this proposal, we predict that $1e^-$ reduction of the trinuclear copper cluster would give a triplet EPR if the coppers ions are ferromagnetically coupled, but no EPR if they are antiferromagnetic coupled at low temp (4.2K)

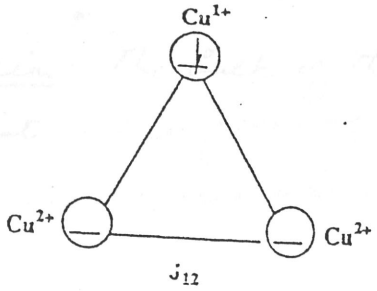

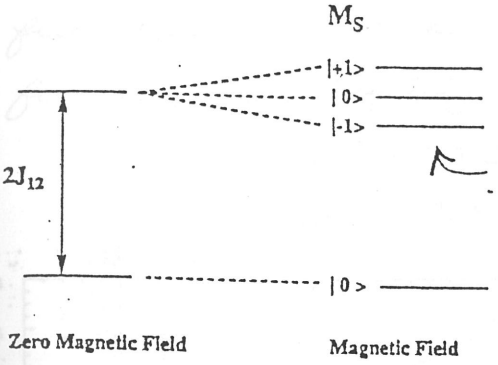

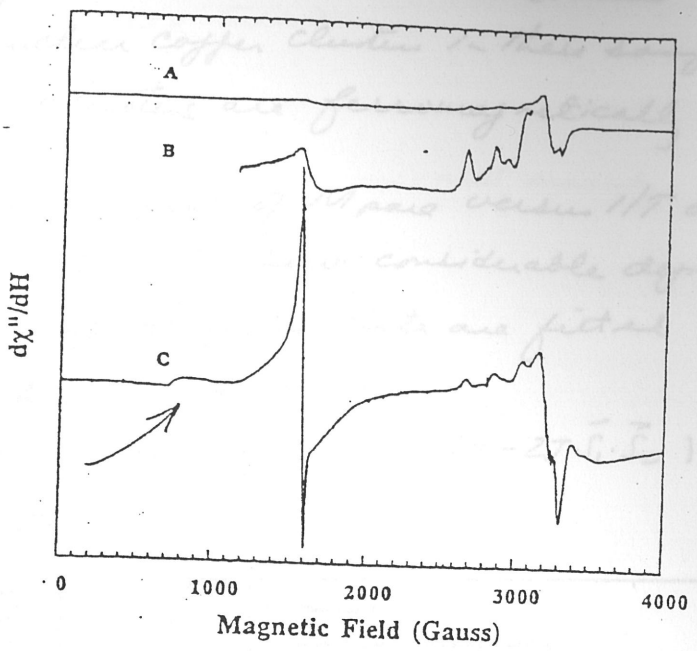

→ Magnetic Susceptibility

Can address the cluster issue most directly by low-temperature magnetic susceptibility measurements

(1) For $J >> k_BT$, only the lower energy spin manifold will be significantly populated. Accordingly, measurement of the saturation magnetization under conditions $(H/T) \rightarrow \infty$ should yield the effective spin of ground level.

(2) M_{para} of the pMMO membranes has been measured at 1.8 K as a function of magnetic field from 0 → 5.5 T. Data obtained fit the Brillouin function with an S_{eff} of 1.44 ± 0.06.

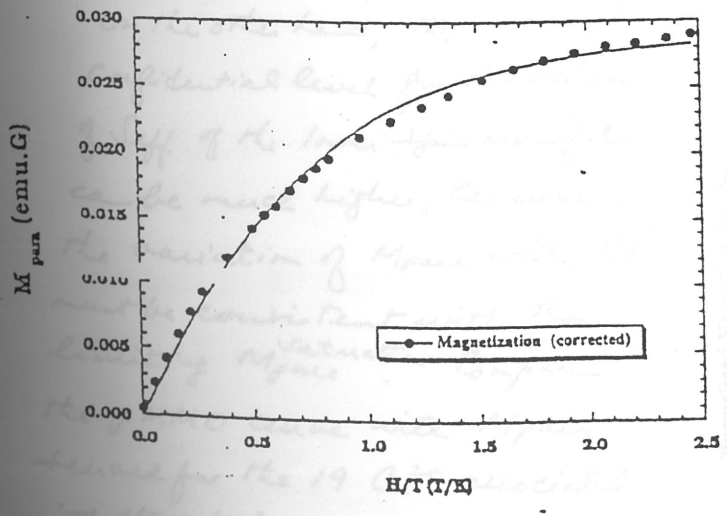

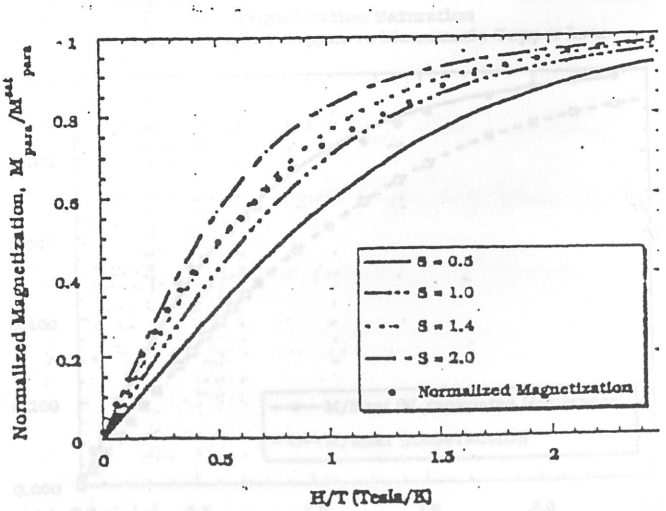

Conclusion: The bulk of the copper ions in the MMO membranes exist in the form of trinuclear copper clusters in these samples!, and the coppers within the clusters are ferromagnetically coupled

(3) Curie Plots: As expected, plots of Mpara versus 1/T over the temperature range 1.8 - 270 K show considerable departure from linearity. When the magnetization data are fitted to ferromagnetic coupling scheme, we obtain

$J \cong +20\ cm^{-1}$ (ferromagnetic $\hat{H} = -2J\vec{S}_1 \cdot \vec{S}_2$)

$D \cong 0.05\ cm^{-1}$

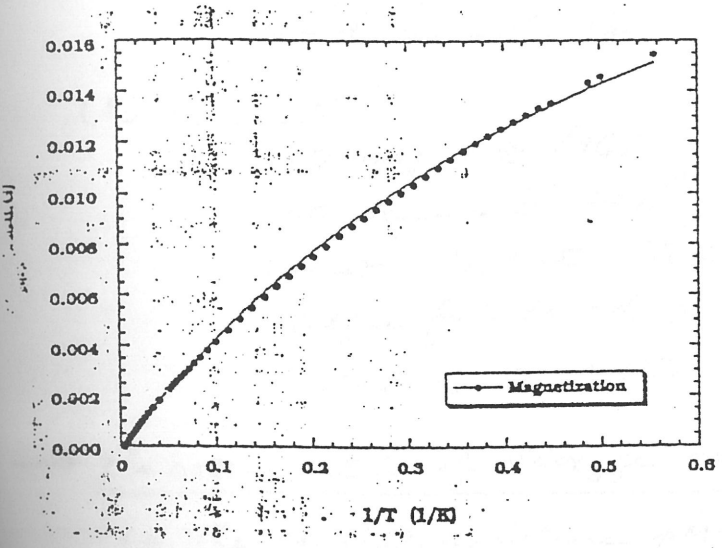

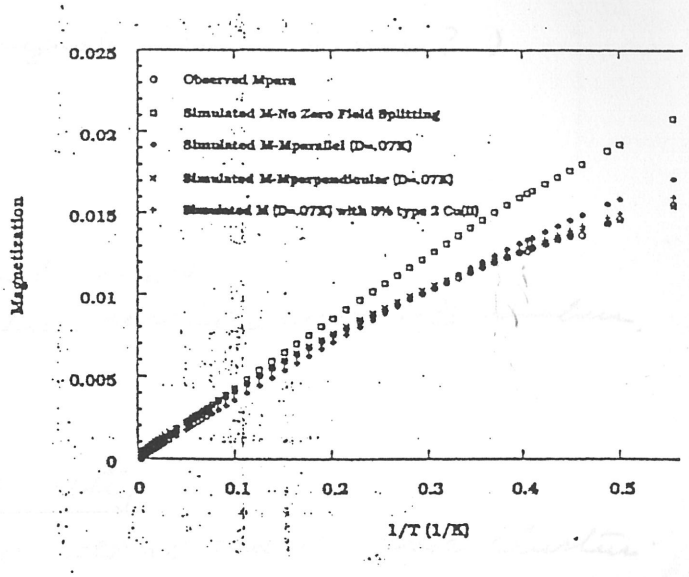

As the temperature is increased, the upper levels of the $S = 3/2$ spin manifold and the $S = 1/2$ levels become populated, so the contribution of these states to the magnetization can be used to infer $D \approx J$. These results need independent confirmation by EPR, because it is not clear that fits to the experimental Mpara can be unique.

On the other hand, the confidential level for the value of Seff of the lower spin manifold can be much higher, because the variation of Mpara with H/T must be consistent with the limiting $M_{para}^{saturation}$. Compare the pMMO curve with Mpara observed for the 19 Cu^{2+} associated with HRG (= histidine rich glycoprotein)

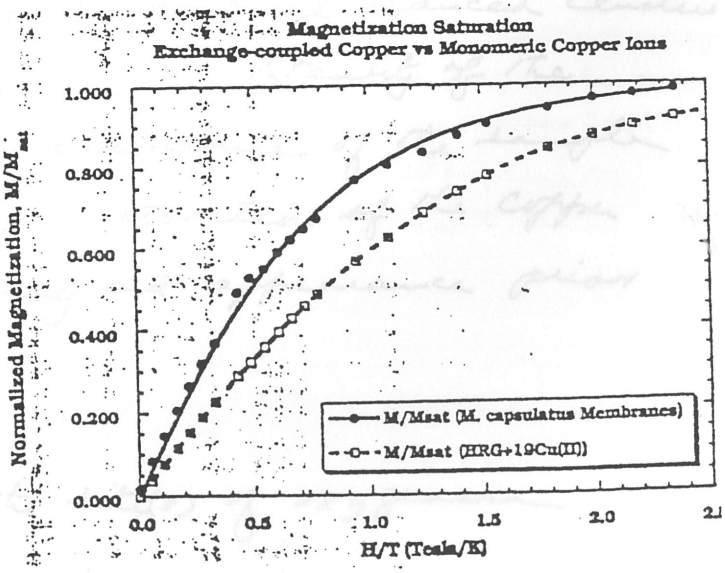

For the HRG + 19 Cu(II) system. EPR clearly indicate that the Copper ions are uncoupled, i.e., they are all type 2.

→ EXAFS

(1) preliminary results on oxidized and semi-met mixed valence samples

(2) Oxidized

2.5 Oxygens @ 1.95Å
1.3 Oxygen @ 2.10Å
Cannot rule out nitrogen 1st shell
Sulfur fits do not produce realistic CN
No discernable Cu–Cu signal (static disorder?)

(3) Semi-met

1.7 Oxygens @ 1.96Å
1.0 oxygens @ 2.06Å
Cannot rule out nitrogen 1st shell
Sulfur fits do not produce realistic coordinate number.
1.5–2 Cu @ 2.55Å

→ The active site(s) of dioxygen chemistry

(1) The correlation between pMMO activity and the copper clusters in these membranes suggests that these clusters might be the active site(s) of the pMMO.

(2) The catalytic role of the copper clusters is also implicated by the reactivity of the partially reduced clusters toward O_2. As noted earlier, anaerobic titration of the membranes by limiting dithionite leads to partially reduced clusters and a substantial decrease in the intensity of the isotropic EPR signal. Upon re-exposure of the samples to air, we observed a full restoration of the copper signal to its original intensity and appearance prior to electron reduction.

Conclusion

Copper clusters most likely the site(s) of oxygenase activity.

→ A possible mechanism

Catalytic Chemistry

A possible mechanism

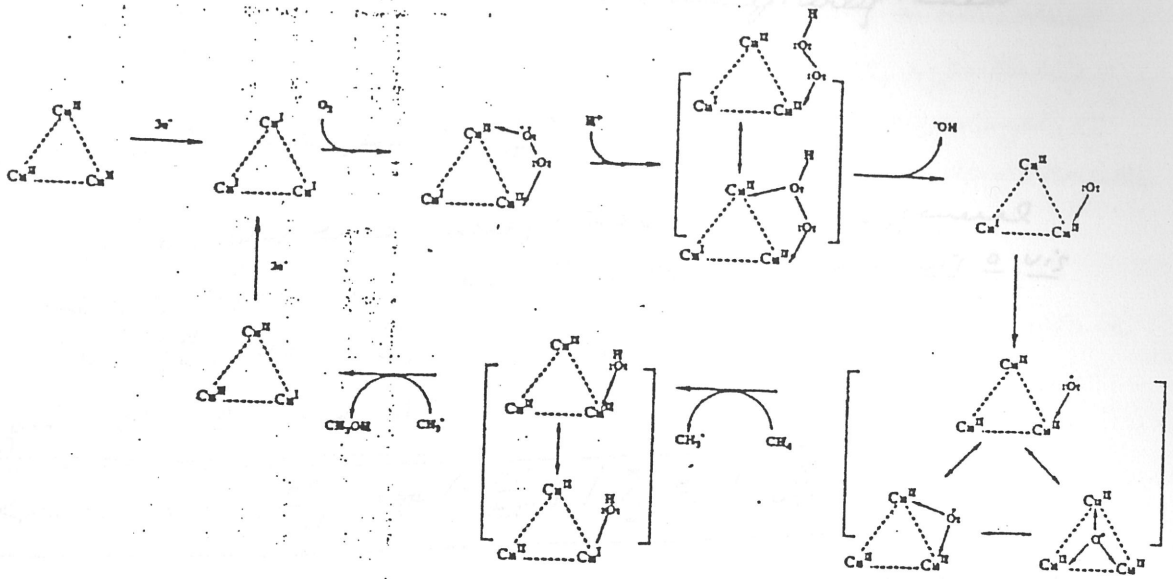

Mechanistic Proposal for Dioxygen and Methane Activation by a Trinuclear Copper Cluster

→ Most studies carried out on membranes enriched in the pMMO. pMMO is overexpressed in these cells under high $[Cu^{2+}]$. Efforts are underway to purify the enzyme toward homogeneity

- Magnetic Susceptibility

Define first Magnetization = magnetic moment of sample / unit vol.

$$M_H(T) = \frac{N_A \langle \mu_H \rangle_T}{V_M} = \frac{N_A \langle \mu_H \rangle_T \rho}{m}$$

where $\langle \mu_H \rangle_T$ = ensemble average of the molecular magnetic moment parallel to H at temperature T and V_M = molar volume

m = molecular mass
ρ = density

$$\text{Molar susceptibility } \chi_H(T) = \frac{N_A \langle \mu_H \rangle_T}{H} = \left(\frac{m}{\rho}\right) \frac{M_H(T)}{H}$$

For each molecule occupying energy state i and oriented with respect to applied magnetic field as follows

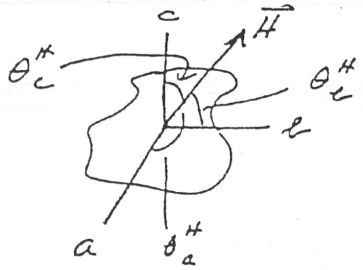

where a, b, c denote the principal axes of the molecular magnetic susceptibility tensor $\ddot{\chi}$

$$\epsilon_i = -\vec{\mu}\cdot\vec{H} \quad \text{and} \quad \mu_H = -\frac{\partial \epsilon_i}{\partial H}$$

μ_H is different for each energy state i, and in general is different for different orientations of molecule w.r.t. $\vec{H}$, i.e., θ_a^H, θ_b^H, θ_c^H.

For a given θ_a^H, θ_b^H and θ_c^H,

$$\boxed{\langle \mu_H \rangle_T = -\sum_i \frac{\partial \epsilon_i}{\partial H} \exp\left(-\frac{\epsilon_i}{kT}\right) \Big/ \sum_i \exp\left(-\frac{\epsilon_i}{kT}\right)}$$

Can define $\langle \mu_{Ha} \rangle_T$, $\langle \mu_{Hb} \rangle_T$ and $\langle \mu_{Hc} \rangle_T$, a quantity that could be measured for a sample wherein all the molecules are oriented

$$\langle \mu_{Ha} \rangle_T = -\sum_i \frac{\partial \epsilon_i}{\partial H_a} \exp\left(-\frac{\epsilon_i}{kT}\right) \Big/ \sum_i \exp\left(-\frac{\epsilon_i}{kT}\right)$$

$$\langle \mu_{Hb} \rangle_T = -\sum_i \frac{\partial \epsilon_i}{\partial H_b} \exp\left(-\frac{\epsilon_i}{kT}\right) \Big/ \sum_i \exp\left(-\frac{\epsilon_i}{kT}\right)$$

$$\langle \mu_{Hc} \rangle_T = -\sum_i \frac{\partial \epsilon_i}{\partial H_c} \exp\left(-\frac{\epsilon_i}{kT}\right) \Big/ \sum_i \exp\left(-\frac{\epsilon_i}{kT}\right)$$

from which we can define the molecular susceptibilities:

$$\bar{\chi}_a(T) = \langle \mu_{Ha} \rangle_T / H_a$$

$$\bar{\chi}_b(T) = \langle \mu_{Hb} \rangle_T / H_b$$

$$\bar{\chi}_c(T) = \langle \mu_{Hc} \rangle_T / H_c$$

Now for any arbitrary orientation

$$\langle \mu_H \rangle_T = -\sum_i \left(\frac{\partial \epsilon_i}{\partial H_a} \cdot \frac{dH_a}{dH} + \frac{\partial \epsilon_i}{\partial H_b} \cdot \frac{dH_b}{dH} + \frac{\partial \epsilon_i}{\partial H_c} \frac{dH_c}{dH} \right) \Big/ \sum_i \exp\left(-\frac{\epsilon_i}{kT}\right)$$

$$= \bar{\chi}_a(T) H_a \cos\theta_a^H + \bar{\chi}_b(T) H_b \cos\theta_b^H + \bar{\chi}_c(T) H_c \cos\theta_c^H$$

$$\frac{\langle \mu_H \rangle_T}{H} = \bar{\chi}_a(T) \cos^2\theta_a^H + \bar{\chi}_b(T) \cos^2\theta_b^H + \bar{\chi}_c(T) \cos^2\theta_c^H$$

• Non-heme iron-oxo proteins (continued)

→ Purple acid phosphatase

* Sources : bovine spleen, rat spleen, human spleen porcine uterine fluid (uteroferrin); also plants + microbial

* Function : catalyzes phosphate ester, thereby regulating the physiological level of inorganic phosphate and phosphorylated metabolites under acidic conditions

* Molecular mass molecular mass 35-40 kD

* Color : purple/pink chromophore in contrast with the greenish color of met Hr & ribonucleotide reductase Visible absorption at 510-550 nm ($\epsilon \sim 4000\ M^{-1}\ cm^{-1}$). Raman studies indicate that absorption arises from tyrosinate-to-iron(III) charge transfer.

* EPR and magnetic susceptibility studies indicate that the oxidized (purple) enzyme contains an antiferromagnetically coupled $(Fe^{III})_2$ unit, and the enzymatically active, reduced (pink) enzyme contains a spin-coupled (weak) mixed valence Fe(III) - Fe(II) cluster, for both the bovine spleen & [uterine/porcine] enzymes. (EPR and $g' = 1.7-1.8$

* Similar to Hr

* On basis of paramagnetic NMR, both histidine and tyrosine ligands are implicated as ligands to Fe-Fe cluster

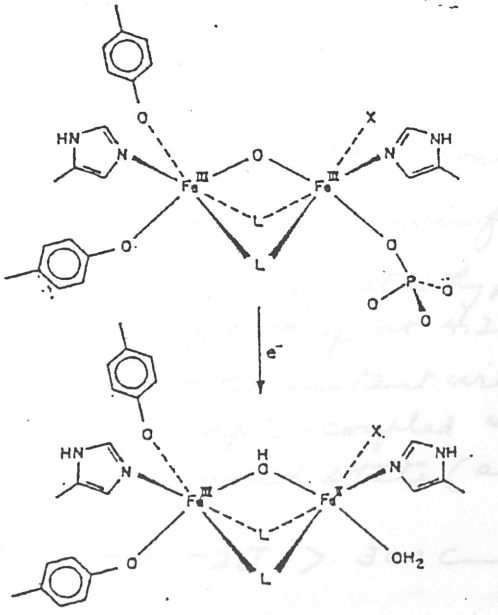

Proposed model for the binuclear iron site of purple and pink bovine spleen FePase and uteroferrin, based on this work and that cited in the text. L indicates possible bridging ligands in addition to a μ-oxo; X indicates unidentified ligand.

* The effect of electron reduction on the absorption, specifically the persistence of the charge transfer transition in the reduced form with almost identical extinction coefficient strongly suggests that tyrosine is coordinated solely to the iron center that remains ferric following reduction. This conclusion is confirmed by resonance Raman studies. (12)

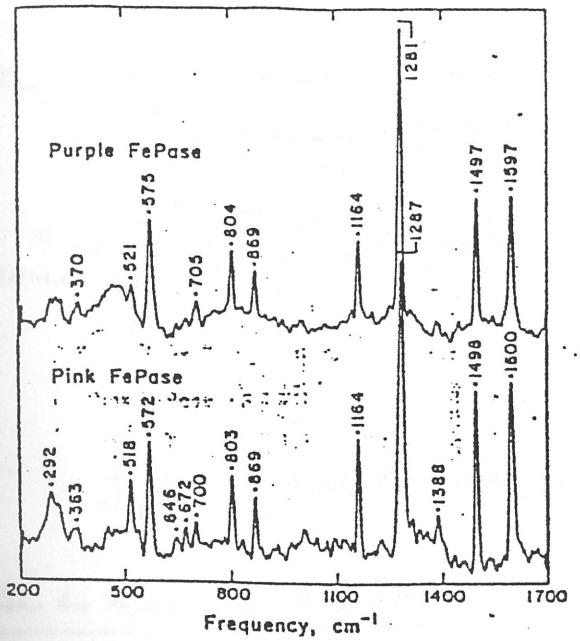

Resonance Raman spectra of 5 mM purple (top) and 2.7 mM pink (bottom) forms of bovine spleen FePase in 10 mM NaOAc buffer, pH 5.0 at 5 °C. Sample temperature was maintained by placing the capillary in the cold-finger of an ice-filled Dewar.[28] Data were collected with use of 514.5-nm excitation, 100-mW incident power, and 140° back-scattering geometry. The spectra shown are an average of 3 scans (purple) and 8 scans (pink) taken at a scan rate of 1 cm^{-1}/s and a slit width of 4–5 cm^{-1} and then subjected to a 13-point smooth.

essentially identical

* Mössbauer spectrum of oxidized bovine spleen FePase

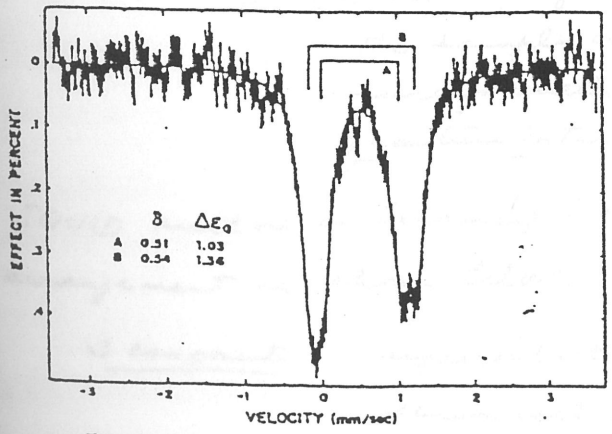

^{57}Fe Mössbauer spectrum at 4.2 K of purple (oxidized) bovine spleen FePase (2 mM in 50 mM NaOAc, pH 5.0). The solid line is a fit to the data with use of the parameters in Table II. Data aquisition time was 47 h.

→ δ and ΔE_Q consistent with high-spin ferric.

→ No magnetic hyperfine splitting at 4.2K observed — consistent with a spin-coupled diamagnetic ground state (also no EPR)

→ $-2J > 300\ cm^{-1}$

$$M_H^{oriented}(T) = \frac{N_A \rho}{m} H \left(\bar{\chi}_a(T) \cos^2\theta_a^H + \bar{\chi}_b(T) \cos^2\theta_b^H + \bar{\chi}_c(T) \cos^2\theta_c^H \right)$$

Define $M_a(T) = \frac{\rho}{m} N_A \bar{\chi}_a(T) \cdot H$

$$M_b(T) = \frac{\rho}{m} N_A \bar{\chi}_b(T) \cdot H$$

$$M_c(T) = \frac{\rho}{m} N_A \bar{\chi}_c(T) \cdot H$$

Then $M_H^{oriented}(T) = M_a(T) \cos^2\theta_a^H + M_b(T) \cos^2\theta_b^H + M_c(T) \cos^2\theta_c^H$

For a powder sample, must average over all possible orientation of the molecules versus the applied magnetic field

$$M_{observed} = \frac{1}{4\pi} \int_0^{2\pi} \int_0^{\pi} \left[M_a(T) \cos^2\theta_a^H + M_b(T) \cos^2\theta_b^H + M_c(T) \cos^2\theta_c^H \right]$$

$\phi \quad \theta \qquad\qquad \sin\theta \, d\theta \, d\phi$

$$= \frac{1}{3} \left[M_a(T) + M_b(T) + M_c(T) \right]$$

How to measure $M_H(T)$

Determined by (1) the force exerted by a magnetic field gradient, usually measured in a Faraday balance

or (2) electric signal induced in a coil when the sample is moved, as in a Faraday susceptometer or SQUID (superconducting quantum interference device)

SQUID method is becoming the standard. The typical arrangement is shown below.

3 components: superconducting solenoid
sensor coil (superconducting)
pick up coil (detector)

The signal induced in the sensor coil as the sample is passed through the sensing coil is detected by the SQUID detector.

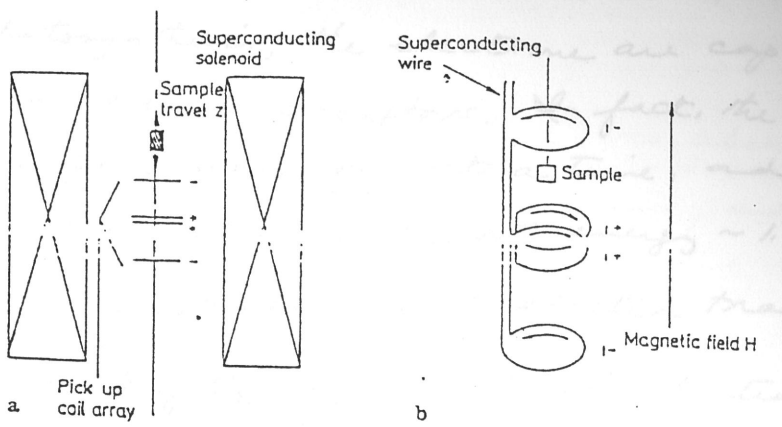

The magnet configuration (a) and the sensor (second-derivative coil) configuration (b) of the MPMS SQUID-susceptometer

- **Photosynthesis and the Photooxidation of Water**

Water splitting, the photolysis of water to produce O_2 and H_2, has long been thought to be a way out of the impending fossil fuel crisis by 2050.

$$2H_2O(liq) \xrightarrow{h\nu} O_2(g) + 2H_2(g)$$

Solar radiation is the obvious candidate for the ultimate energy source, but water cannot be photolyzed directly by the relatively low-energy visible photons ($\lambda > 300$ nm) that penetrate the earth's atmosphere.

On the other hand, the photooxidation of water to produce O_2 and reduced substances with reduction potentials similar to that of H_2, is accomplished efficiently using sunlight by plants and algae. To produce a molecule of O_2 from water requires the removal of four electrons from two H_2O molecules (Note reverse of respiration!):

$$2H_2O(l) \longrightarrow O_2(g) + 4H^+(g) + 4e^-$$

If the electrons and H^+ ion combine, we can complete the reaction by $4H^+(aq) + 4e^- \longrightarrow 2H_2(g)$. However,

in plant photosynthesis, the electrons are captured by other low potential electron acceptors. In fact, the electrons are transferred from water one at a time, and the photons are absorbed by chlorophyll with energy ~ 1.8 eV. Since ΔG° for the overall reaction of electron transport corresponds to 114 kcal / mol of O_2 . or ~ 1.23 eV / electron transferred, there is sufficient energy to accomplish this. Despite this, plants have evolved a scheme whereby this one-electron oxidation is accomplished by two light reactions acting in series.

→ The Z-scheme of photosynthetic electron transport

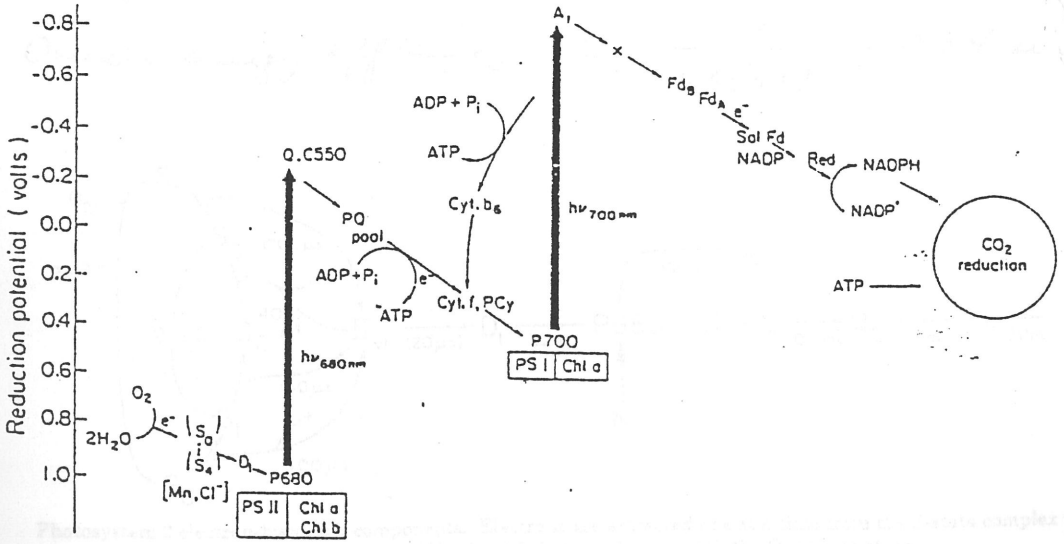

The Z scheme of electron transport for higher plant photosynthesis. The two light reactions of photosystem 1 and photosystem 2 are thought to operate in series, connected by a portion of the electron-transport chain involving quinones (Q, PQ), cytochrome f (Cyt f), and the copper protein, plastocyanin (PCy). Strong oxidants produced by photosystem 2 remove electrons from the Mn-containing complex that results in water oxidation. Photosystem 1 produces powerful reductants that donate electrons to ferredoxin (Fd) NADP and are ultimately responsible for CO_2 reduction.

(1) Two photosystems : PS II (P680)
PS I (P700)

(2) Photooxidation of water begins with photoexcitation of P680.
P680 consists of a chlorophyll pair

$$P680 \xrightarrow{h\nu} P680^* \longrightarrow P680^+ + e^-$$

The source of the oxidizing power is in the reaction centers of photosystem II.

(3) P_{680}^+ is returned to P_{680} via abstraction of an electron from D_1, a tyrosine, and the tyrosine radical is subsequently reduced by an electron from the water-splitting complex. Thus, each photon that activates photosystem II leads to the transfer of a single electron from the water-splitting complex to the intermediate electron carriers, and a second photon entering photosystem I transmits the electron to the terminal acceptors in intact chloroplasts.

(4) 8 photons are required for each O_2 evolved. 4 photons are absorbed in photosystem I, and four photons in photosystem II.

(5) Overall energy efficiency $\leq \frac{1.23}{2 \times (1.8)} = 0.34$ or 34%.

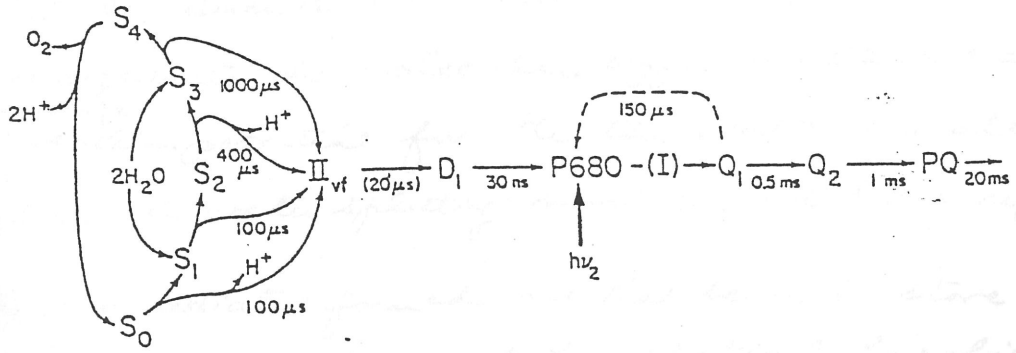

Photosystem 2 electron-transport components. Electrons are extracted one at a time from the S-state complex to advance it by stages through its cycle. A probable pattern of H^+ release is indicated along with the O_2-release stage.

(6) The oxidizing equivalents following successive photoexcitations are stored and accumulated at the water-splitting complex for water oxidation (after four oxidizing equivalents)

→ The water-splitting complex is a Mn cluster

(1) The essential involvement of manganese in water oxidation was foreshadowed by the observation by Brion in 1937 that plants or algae deprived of Mn in their growth media lost the ability to evolve O_2. addition of Mn to the growth medium resulted in restoration of H_2O oxidation in 30 min.

(2) There are two pools of Mn in higher plant or algae.
(a) a reservoir of Mn^{2+} that is weakly membrane bound. This pool of manganese can be removed essentially completely by cell rupture and washing pigmented membranes with EDTA. These washed chloroplast membranes still have high level of O_2 evolution, when artificial electron acceptors such as ferricyanide are used (Hill reaction)

(b) The second pool of manganese is tightly bound, consisting of between 6 and 8 atoms per photosynthetic electron-transport chain. About 2/3 of this pool can be released by alkaline-Tris washing or hydroxylamine extraction, and this release correlates with a loss of Hill reaction activity. The remaining 1/3 of the Mn is very tightly bound, and its presence is not correlated with O_2 evolution.

(3) Manganese is an attractive element for the water-splitting complex, because of its multiple oxidation states, some of which involve relatively high reduction potentials. Since the standard reduction potential necessary to oxidize water to molecular oxygen is 0.82 volt at pH 7, the average reduction potential for the three intermediates involved in water splitting must be ~0.8 V or higher.

(4) The intermediates formed and that serve to store the oxidizing equivalents must be relatively long-lived, because photons arrive in a statistical fashion, not in quanta of 4. Also the quantum efficiency of the Hill reaction remains high even to very low light flux.

(5) Direct evidence for long-lived intermediates came from experiments of Joliot (Photochem. Photobiol 10, 309 (1969)) & coworkers. They applied a train of brief (10 μs) saturating flashes of light to chloroplasts or O_2-evolving algae (and adapted) initially in the dark. Significant O_2 yields appear only after the third flash, and subsequent flashes in the

train produce further O_2 pulses whose amplitude oscillates with a period of four flashes. After 25-30 flashes, the oscillations damp out to give a uniform steady state yield

KOK et al. MODEL OF PHOTOSYNTHETIC O_2 EVOLUTION

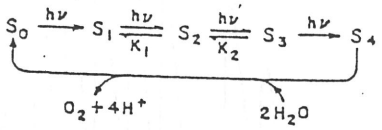

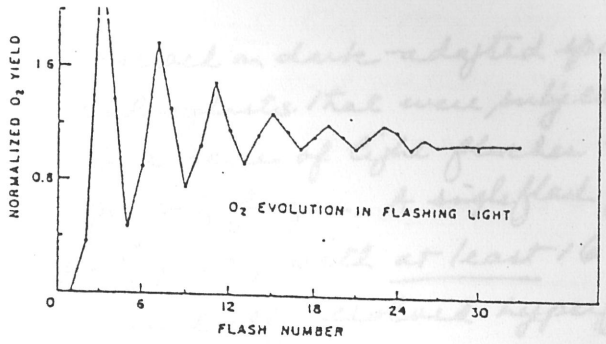

(6) Interpretation of flash-induced O_2-yield oscillations

Kok's S-state scheme (B. Kok, B. Forbush, & M. McGloin, Photochem. Photobiol. 11, 457-475 (1970)).

Proposal

(a) Water splitting complex exists in a set of five states, S_0 through S_4, representing successive stages of oxidation, or advancement, of the O_2-evolution complex.

(b) To account for the high-yield of O_2 on the third flash, it was proposed that S_1 as well as S_0 is stable in the dark, and that they are normally present initially in the ratio of $[S_1]/[S_0] = 3$ following dark adaptation

(c) Occasional double hits (5-10%) and misses (10%) result in dephasing of the array of S-state complexes in a macroscopic sample.

(d) S_2 and S_3 are powerful oxidants or species involving partially oxidized water. They are nevertheless stable for periods of the order of minutes at room temperature. They relax back to S_1 if no further photon activation occurs during this interval (with decay constants of k_1 and k_2 in Kok scheme).